# High Velocity Operation of the Thermally Choked Ram Accelerator

by

Joshua E. Elvander

A thesis submitted in partial fulfillment
of the requirements for the degree of

Master of Science in Aeronautics and Astronautics

University of Washington

1997

# High Velocity Operation of the Thermally Choked Ram Accelerator

by

Joshua E. Elvander

A thesis submitted in partial fulfillment
of the requirements for the degree of

Master of Science in Aeronautics and Astronautics

University of Washington

1997

Approved by _____
(Chairperson of the Supervisory Committee)

Program Authorized
to Offer Degree _____Aeronautics and Astronautics_____

Date _____

In presenting this thesis in partial fulfillment of the requirements for a Master's degree at the University of Washington, I agree that the Library shall make its copies freely available for inspection. I further agree that extensive copying of this thesis is allowable only for scholarly purposes, consistent with "fair use" as prescribed in the U.S. Copyright Law. Any other reproduction for any purposes or by any means shall not be allowed without my written permission.

Signature _____

Date_____

University of Washington

Abstract

HIgh Velocity Operation of the Thermally Choked Ram Accelerator

by Joshua E. Elvander

Chairperson of the Supervisory Committee
Professor Adam P. Bruckner
Department of Aeronautics and Astronautics

The ram accelerator is a chemically-based hypervelocity launcher based on the same gasdynamic operating principles as a supersonic ramjet. Several potential applications have been identified, many of which are dependent on the high velocities theoretically possible using the device, which can range to as high as 8 km/s. The highest velocity observed to date in a ram accelerator is 2.7 km/s. The motivation for the research presented is to enable higher velocities to be realized. A theoretical analysis of the subdetonative, thermally choked ram accelerator is presented, and methods to achieve high acceleration are identified: increase the fill pressure of the ram accelerator tube; increase the tube's cross-sectional area; decrease the projectile mass; or increase the thrust available from the propellant mixture, by either increasing the nondimensional heat release or decreasing the entrance freestream Mach number. Each of these methods is analyzed. Mixture maps are presented as a technique to visualize the coupled relationship of heat release and Mach number and to obtain high accelerations in a relatively small number of experiments. Results of existing work to identify geometric effects on projectile performance are reviewed, culminating in a reduced mass projectile which masses two-thirds as much as a standard design yet can match performance in the thermally choked propulsion regime. Mixture maps were employed using methane/oxygen and methane/oxygen/helium mixtures to obtain high performance propellant mixtures for the first, second and third stages. Repeatable accelerations as high as

38,000 *g's* over 2 m and 35,000 *g's* over 6 m were observed, accelerating a 50 gm aluminum alloy projectile to 2404 m/s in 6 m. The results are analyzed and discussed, and presented as validation of the technique developed to obtain high velocity operation of the thermally choked ram accelerator.

# Table of Contents

*Page*

*Page*

# List of Figures

*Number* *Page*

*Number* *Page*

*Number* *Page*

# Nomenclature

| | |
|---|---|
| $A$ | cross-sectional tube area |
| $a$ | sound speed |
| $c_p$ | specific heat at constant pressure |
| $c_v$ | specific heat at constant volume |
| $F$ | thrust |
| $h$ | enthalpy |
| $M$ | Mach number |
| $p$ | pressure |
| $Q$ | nondimensional heat release |
| $R$ | specific gas constant |
| $T$ | temperature |
| $u$ | velocity |
| $V_{CJ}$ | Chapman-Jouguet detonation velocity |

## Greek

| | |
|---|---|
| $\Delta q$ | heat release of combustion |
| $\gamma$ | ratio of specific heats |
| $\rho$ | density |
| $\tau$ | nondimensional thrust |

## Subscripts

| | |
|---|---|
| *1* | upstream freestream condition |
| *2* | downstream freestream condition |
| *CJ* | Chapman-Jouguet |

# Acknowledgements

I would like to thank certain individuals whose efforts contributed to the quality of the work presented here, and to whom I am extremely grateful. Dr. Adam P. Bruckner, my adviser, provided continuous support for the experiments and a great deal of freedom and encouragement to pursue my own ideas. Dr. Carl Knowlen advised me on various aspects of ram acceleration and the nature of engineering research, and provided many enlightening discussions and essential guidance during the experiments.

I would also like to express my appreciation to the ram accelerator students. Andrew Higgins provided helpful advice and assistance, particularly in the initial experiments, and helped to train me in the ways of ram, along with Tom Imrich, whose projectile geometry experiments paved the first steps toward high velocity operation. Jesse Stewart, Eric Schultz, David Buckwalter, Chris Bundy and Ryan Schwab all helped with many varied aspects of this effort, from assisting with experiments to providing fresh perspectives on my writing.

Thanks are due to Ron Musgrave and Dan Skow of the University of Washington Physics Instrument Shop, who manufactured all the projectiles used in the experiments with a high degree of precision, repeatability and attention to detail.

Finally, I would like to acknowledge Army Research Office, which financially supported this research under grants AASERT DAAH04-93-G-0389 and DAAL03-02-G-100, the latter under the monitoring of David Mann.

This research thesis is but a small portion of my adventure in graduate study at the University of Washington, and hopefully my time here will not be judged solely on its content. Space considerations prevent me from acknowledging all the people who contributed significantly to my experience. They know who they are. They have my heartfelt thanks, respect and admiration.

# 1. Introduction

The ram accelerator is a device for accelerating projectiles to very high velocities based on the same gasdynamic properties of a conventional ramjet.[1] A ram accelerator projectile travels through a tube filled with premixed fuel and oxidizer at high pressure (Fig. 1.1). The ram projectile has a conical nose and tapering rear section similar in shape to a ramjet's centerbody, and the inner diameter of the tube is analogous to the ramjet's outer cowling. The projectile is initially launched into the tube at supersonic speed, and a system of shocks is established leading to combustion behind the projectile which produces a pressure wave that accelerates it to high velocities.

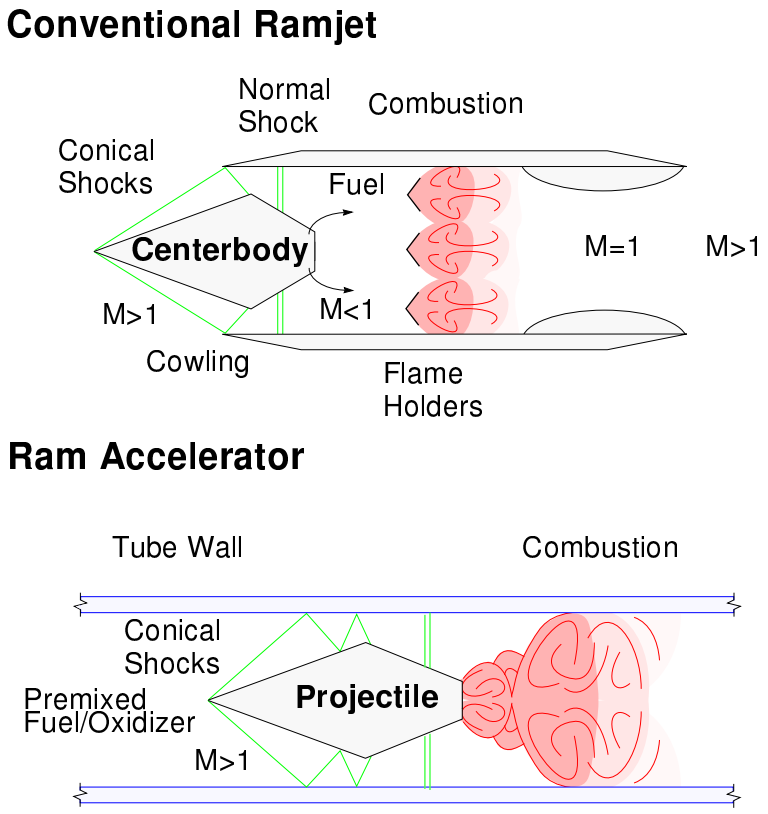


**Figure 1.1: Comparison of supersonic ramjet and ram accelerator.**

Although the ram accelerator shares operating principles with a ramjet, it has some distinctions which make it a unique propulsion system. It is chemically based and utilizes the surrounding medium as its working fluid, as in ramjets and turbojets, but it is not air-breathing. Its working fluid consists of both the oxidizer, which in airbreathing vehicles is the oxygen obtained from the air, and the fuel, which in airbreathing vehicles is carried on board. The oxygen/fuel mixture is contained at high pressure in the tube through which the ram accelerator projectile travels. When considering the ram accelerator, this entire tube must be taken into account. Sutton uses the term *duct* propulsion instead of airbreathing,[2] which is perhaps more appropriate.

In many ways the ram accelerator is more like a gun than a traditional chemical propulsion system such as a rocket, in that a projectile starts at one end of a long tube and

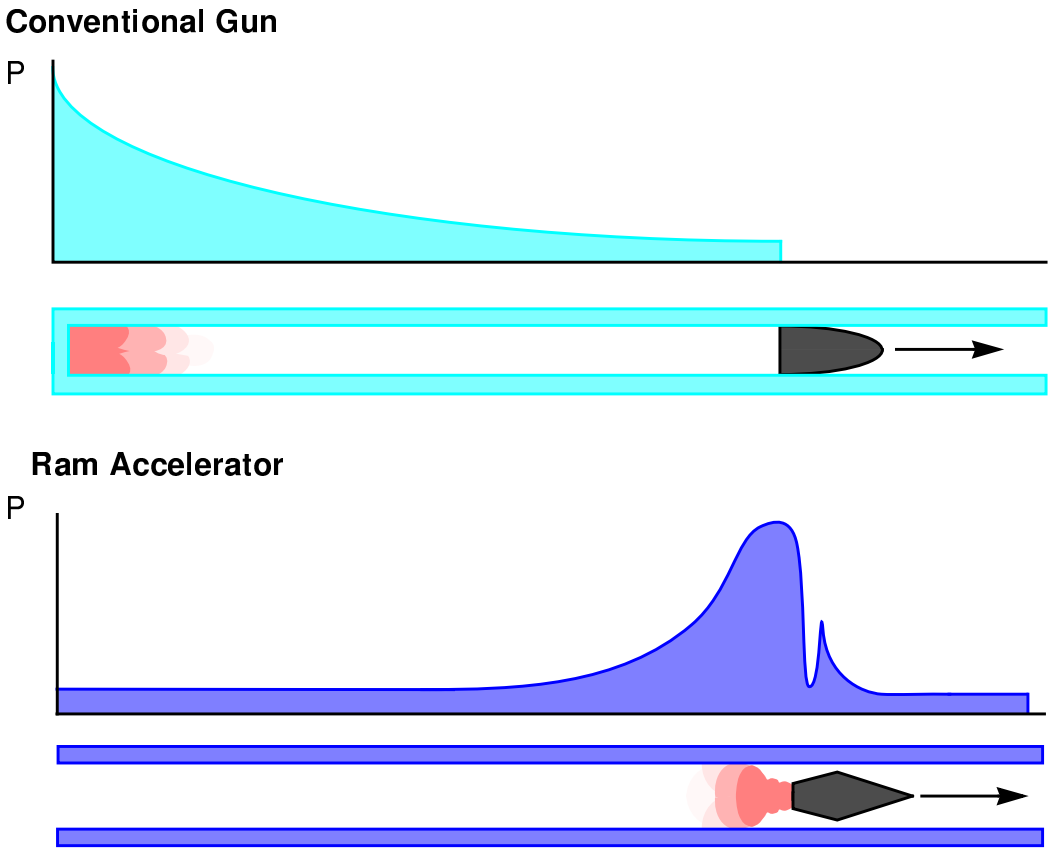


**Figure 1.2: Comparison of conventional gun and ram accelerator.**

exits from the muzzle at very high velocities. In a gun, however, the pressure is highest at the breech and drops as the projectile moves down the tube (Fig. 1.2). In a ram accelerator a pressure wave is established which is always behind the projectile. The projectile "surfs" this pressure wave down the length of the tube. The ram accelerator carries no fuel on board and takes its energy from the medium through which it travels, utilizing the properties of supersonic duct flow to compress and burn the mixture behind the projectile.

Conceived by Hertzberg, Bruckner, and Bogdanoff at the University of Washington (UW) in 1983, the ram accelerator was first experimentally demonstrated by the UW group in 1986.[1] They observed that projectiles accelerate both below and above the Chapman-Jouguet detonation speed ($V_{CJ}$) of the combustible mixture through which the projectile travels, and described projectile performance based on this criterion as either subdetonative or superdetonative.[3] Figure 1.3 shows an experiment where the projectile

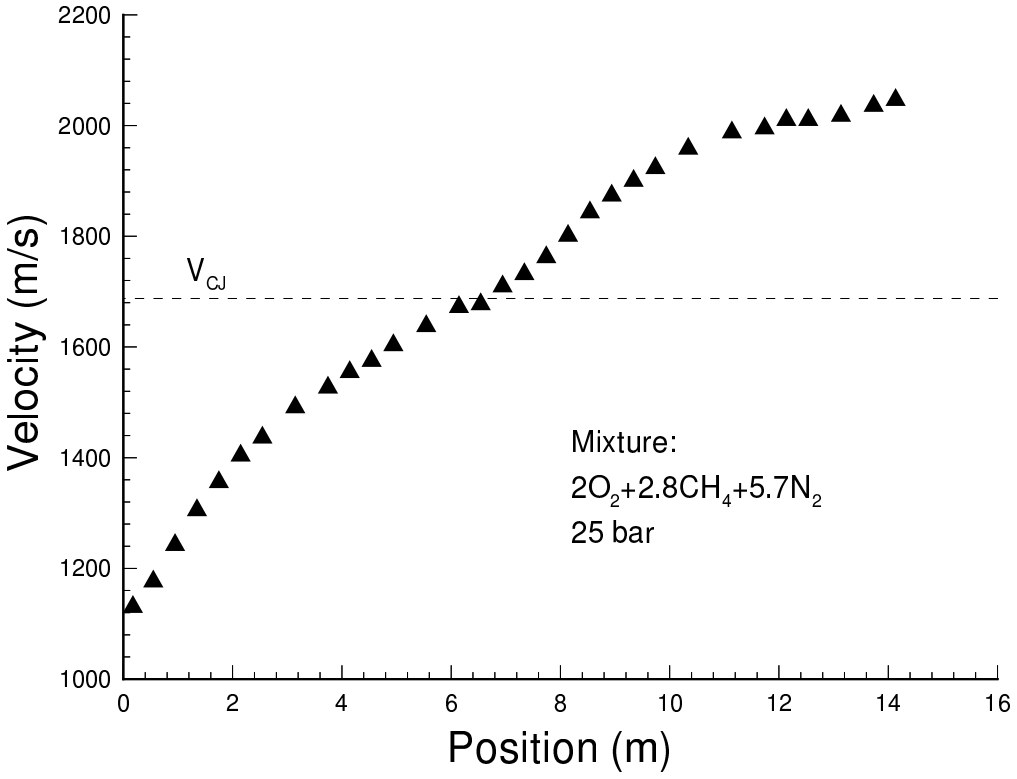


**Figure 1.3: Experimental results showing smooth transition from subdetonative to superdetonative performance.**

smoothly transited from subdetonative to superdetonative velocities. These propulsion modes have been extensively studied, and several different models of ram accelerator operation have been proposed,[3] which take into account the nature of the flow past the projectile and the it's speed relative to $V_{CJ}$.

At subdetonative speeds, a system of conical and normal shocks attached to the projectile's nose decelerates the flow to subsonic speeds behind the point of maximum occlusion of the projectile, referred to as its throat (Figure 1.4). Often, the flow becomes

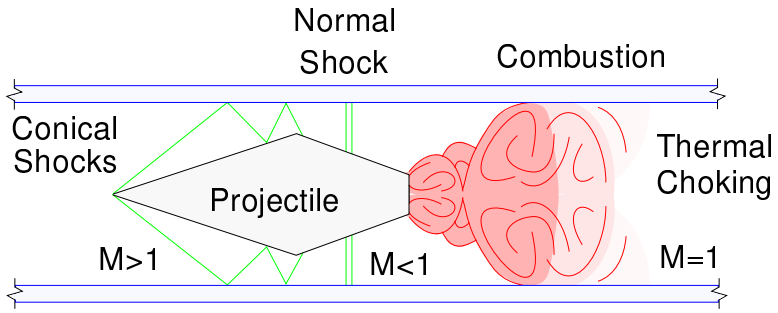


**Figure 1.4: Thermally choked ram accelerator propulsion mode.**

thermally choked behind the projectile base due to combustion; when this happens, the projectile is said to be in the thermally choked mode of combustion. From one-dimensional flow theory, a model of the flow and resulting projectile performance can be developed based on the assumption that this thermal choking occurs at the full tube area behind the base. This model will be discussed in detail in Chapter 2. Note that thermal choking need not occur at subdetonative speeds; it is possible for the flow to remain unchoked behind the projectile. When the performance agrees with theory, however, the flow is usually assumed to be thermally choked, and the subdetonative and thermally choked descriptors have become synonymous. Rigorously speaking they are not.

The velocity range from approximately $0.9V_{CJ}$ to $1.1V_{CJ}$ is referred to as the transdetonative velocity regime. In this operating mode, thermally choked theory is no longer valid.

In the superdetonative mode of operation the flow around the projectile is continuously supersonic (Fig. 1.5) Recent research indicates that projectile speeds on the

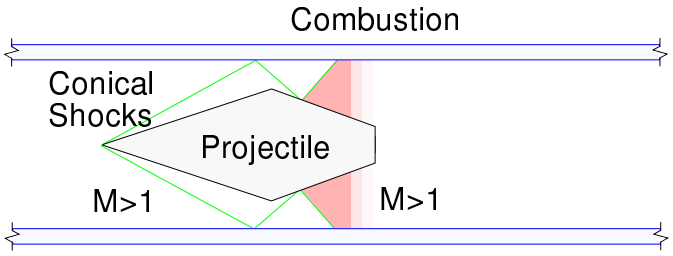


**Figure 1.5: Superdetonative ram accelerator propulsive mode.**

order of $1.5V_{CJ}$ are possible in the superdetonative operating mode, corresponding to about 6 km/s for highly reactive propellant mixtures.[4] All the research described here involved projectile speeds below $V_{CJ}$, and the flow past the projectile is always assumed to be thermally choked.

By varying the mixture through which the projectile travels, it is possible to tailor the acceleration to specific needs. In addition, the ram accelerator can be scaled up or down in size favorably, compared to conventional guns.[5] These features make the ram accelerator an attractive candidate for a variety of applications, such as boosting payloads to orbit, high velocity impact testing and tactical and strategic defense.[6,7] Finally, the aerothermodynamics involved in ram acceleration could potentially provide insights into the nature of oblique detonation waves and the phenomena required to make scramjets a realizable technology.

The variety of uses of ram accelerators has prompted research at many institutions around the world. A 120 mm facility is in operation at the Army Research Laboratory (ARL) in Aberdeen, Maryland.[5] The Institute de Recherches Franco-Allemand de Saint-Louis (ISL) in Saint Louis, France, operates 30 mm and 90 mm facilities.[8,9] In Japan, a 25 mm ram accelerator is being developed at the Institute for Fluid Sciences (IFS) at Tohoku University in Sendai, a 15 mm x 20 mm rectangular facility is in operation at Hiroshima University (HU) in Hiroshima,[10,11] and a 22 mm facility is under construction

at Saitama University (SU) in Saitama. Ram accelerators are also being developed at the Aerodynamics Research and Development Center (ARDC) in Mianyang, China and the Seoul National University (SNU) in Seoul, Korea. Figure 1.6 shows a map indicating

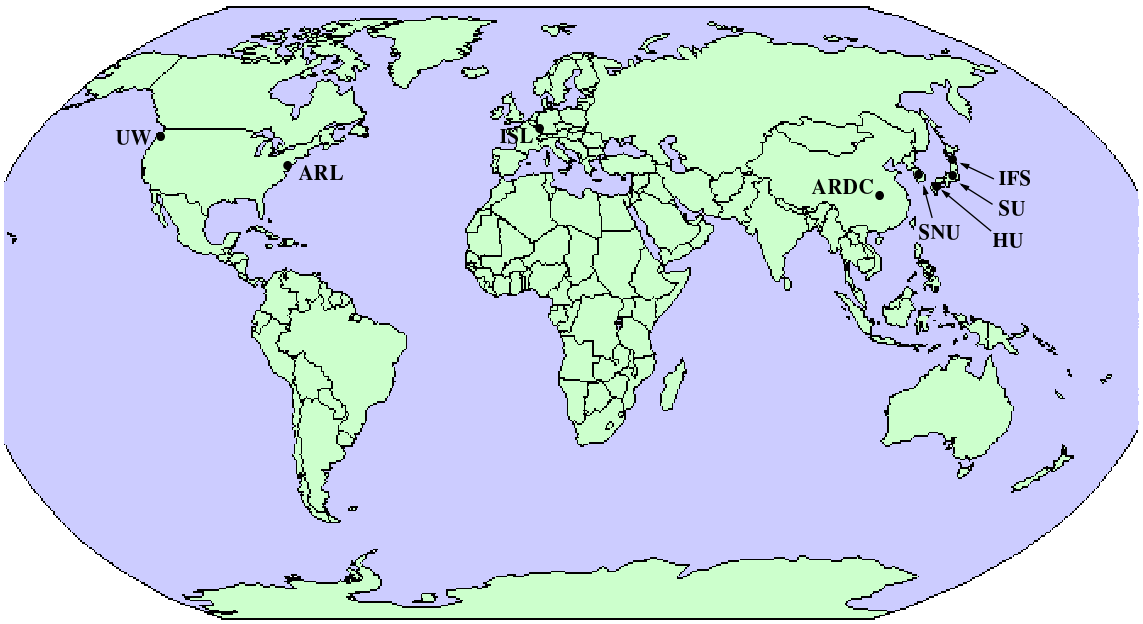


**Figure 1.6: Ram accelerator facilities.**

where these ram accelerators are located. In addition to these experimental facilities, ram accelerators have been the subject of several analytical and computational fluid dynamics papers.

To date, the record velocity achieved by a ram accelerator is 2.7 km/s, achieved by the UW in 1991. Many of the applications listed above have high velocity as one of their main criteria. The motivation for the research presented is attaining the higher velocities that are theoretically possible. In this thesis, the quasi-one dimensional theory of thermally choked, subdetonative ram accelerator operation is discussed and analyzed to determine ways to increase speed, and a technique will be developed to attain higher velocities in a relatively small number of experiments. Experiments validating that technique are then presented, followed by a discussion of results and conclusion.

# 2. Theoretical Model of the Thermally Choked Operating Mode

It is possible to derive a closed form, analytical model of subdetonative ram accelerator performance. Considerable effort has been put forth in recent years to computationally predict superdetonative performance, and it has yielded several highly sophisticated models, but these routines are hampered by the effects of real gas behavior at high pressures and temperatures and the lack of kinetic rate data at the conditions in the combustion zone at hypersonic Mach numbers.[4]

Closed form analysis of the thermally choked ram accelerator is possible via a "blackbox" model that only takes into account the state of the gas upstream and downstream of the projectile. It is also possible to numerically solve a quasi-one-dimensional flow field model that treats the flow around the projectile as isentropic flow with the exception of a normal shock. The blackbox model, although simplistic, has been proven to accurately model subdetonative ram accelerator performance, while the flow field model has been used to predict the operational envelope of the ram accelerator.[12,13] For the purpose of obtaining high velocities in the thermally choked propulsion mode, the blackbox model is more appropriate and will be discussed in the present section.

## 2.1 The "Blackbox" Model

The thrust acting on the projectile can be uniquely determined by flow conditions upstream of the projectile and at the point of thermal choking by assuming thermally choked flow in the entire tube area behind the ram accelerator projectile. If the flow past the projectile is modeled as a one dimensional control volume (Fig. 2.1), the *only* flow conditions which are relevant are those at the entry and exit to the control volume, referred to as conditions 1 and 2. In addition, if the thermally choked flow is assumed to be in equilibrium, then the flow at condition 2 can be determined via equilibrium chemistry. Since the model only takes into account conditions upstream and downstream of the

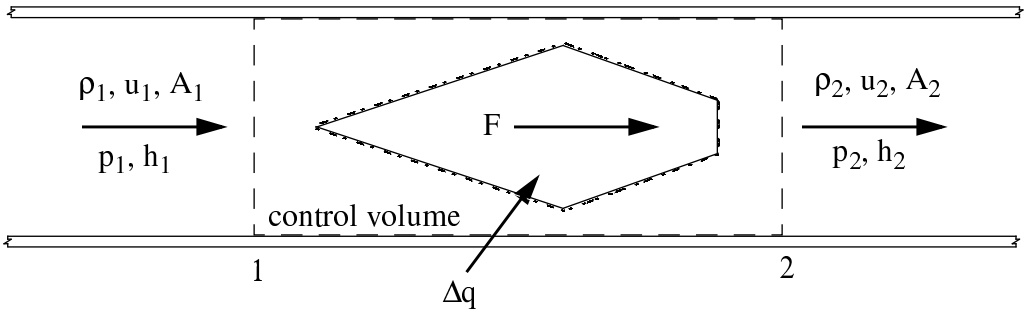


**Figure 2.1: One dimensional control volume for the "blackbox" model of the thermally choked operating mode.**

projectile, information about the projectile shape and its effect on the flow is not necessary, hence the term "blackbox."

The blackbox model can be derived from the continuity equations of mass, momentum and energy:

$$\rho_1 u_1 A_1 = \rho_2 u_2 A_2 \tag{2.1}$$

$$p_1 A_1 + \rho_1 A_1 u_1^2 + F = p_2 A_2 + \rho_2 A_2 u_2^2 \tag{2.2}$$

$$h_1 + \frac{u_1^2}{2} + \Delta q = h_2 + \frac{u_2^2}{2} \tag{2.3}$$

where $\rho$, $u$, and $A$, are, respectively, the density, velocity and cross-sectional area of the flow, and $F$, $h$, and $\Delta q$ are the thrust acting *on* the control volume, the enthalpy, and the heat of combustion of the flow.

The derivation makes the assumptions that the gas through which the projectile moves is ideal. This allows the use of the equation of state for an ideal gas and the relation for the sound speed, $a$:

$$p = \rho RT \tag{2.4}$$

$$a = \sqrt{\gamma RT} \tag{2.5}$$

where $R$ is the specific gas constant, $\gamma$ is the ratio of specific heats and $T$ is the temperature. Finally, the following relations are also used:

$$M = \frac{u}{a} \tag{2.6}$$

$$R = c_p - c_v \tag{2.7}$$

where $M$ is the Mach number of the flow and $c_p$ and $c_v$ are the specific heats of the gas at constant pressure and volume, respectively.

Starting with the equation of momentum conservation (Eqn. 2.2) and using the definition of the Mach number and the fact that the tube cross-sectional area does not change, so $A_1 = A_2$, a nondimensional thrust parameter can be defined:

$$\frac{F}{p_1 A_1} = \frac{p_2}{p_1} - 1 + \frac{\rho_1 M_2^2 a_2^2}{p_1} + \frac{\rho_1 M_1^2 a_1^2}{p_1} \tag{2.8}$$

Invoking the equation of state and sound speed:

$$\frac{F}{p_1 A_1} = \frac{p_2}{p_1}(1 + M_2^2 \gamma_2) - (1 + M_1^2 \gamma_1) \tag{2.9}$$

If the same relations are used with the conservation of mass equation (Eqn. 2.1), again noting that $A_1 = A_2$. some algebra yields:

$$\frac{P_1}{R_1 T_1} M_1 \sqrt{\gamma_1 R_1 T_1} = \frac{P_2}{R_2 T_2} M_2 \sqrt{\gamma_2 R_2 T_2} \tag{2.10}$$

which can be simplified to:

$$\frac{p_2}{p_1} = \frac{M_1}{M_2}\sqrt{\frac{\gamma_1 R_2 T_2}{\gamma_2 R_1 T_1}} \tag{2.11}$$

Looking now to the equation of conservation of energy (Eqn. 2.3), the heat release due to combustion can be nondimensionalized by defining a parameter $Q$ such that $Q = \Delta q/c_{p1}T_1$ which gives:

$$\frac{h_1}{c_{p1}T_1} + \frac{u_1^2}{2c_{p1}T_1} + Q = \frac{h_2}{C_{p1}T_1} + \frac{u_2^2}{2c_{p1}T_1} \tag{2.12}$$

Applying the relations for the Mach number and the specific gas constant yields, after some algebra:

$$\frac{T_2}{T_1} = \frac{c_{p1}}{c_{p2}}\left[\frac{\frac{h_1}{c_{p1}T_1} + M_1^2\frac{\gamma_1 - 1}{2} + Q}{\frac{h_2}{c_{p2}T_2} + M_2^2\frac{\gamma_2 - 1}{2}}\right] \tag{2.13}$$

Eqns.(2.11) and (2.13) can now be substituted into Eqn. 2.9 to yield an equation for the nondimensionalized thrust. This thrust is often denoted by the symbol $\tau$:

$$\tau = \frac{F}{p_1 A} = \frac{M_1}{M_2}\sqrt{\frac{\gamma_1 R_2}{\gamma_2 R_1}\frac{c_{p1}}{c_{p2}}\left[\frac{\frac{h_1}{c_{p1}T_1} + M_1^2\frac{\gamma_1 - 1}{2} + Q}{\frac{h_2}{c_{p2}T_2} + M_2^2\frac{\gamma_2 - 1}{2}}\right](1 + M_2^2\gamma_2) - (1 + M_1^2\gamma_1)} \tag{2.14}$$

After some algebraic manipulation, Eqn (2.14) simplifies to:

$$\tau = \frac{F}{p_1 A} = \frac{M_1}{M_2}\frac{\gamma_1}{\gamma_2}\sqrt{\left[\frac{\gamma_2 - 1}{\gamma_1 - 1}\right]\left[\frac{\frac{h_1}{c_{p1}T_1} + M_1^2\frac{\gamma_1 - 1}{2} + Q}{\frac{h_2}{c_{p2}T_2} + M_2^2\frac{\gamma_2 - 1}{2}}\right]}(1 + M_2^2\gamma_2) - (1 + M_1^2\gamma_1) \qquad (2.15)$$

Note that the assumption of a calorically perfect gas has not been made in this derivation so far. At the temperatures resulting from the chemically reacting flow, $c_p$ is not constant; however, it will be assumed that it does not vary significantly. This assumption carries implicitly for $c_v$ as well. Making these assumptions, the relation $h = c_p T$ can be applied.

Finally, it can also be shown that $\gamma$ does not vary much, so $\gamma_1 = \gamma_2$. Noting these assumptions, and taking into account the fact that for thermally choked flow the flow exiting the control volume is sonic ($M_2 = 1$) yields:

$$\tau = \frac{F}{p_1 A} = M_1\sqrt{\frac{2}{(\gamma + 1)}\left(1 + \frac{\gamma - 1}{2}M_1^2 + Q\right)} - (1 + M_1^2\gamma) \qquad (2.16)$$

Equation (2.16) is the thrust equation for the thermally choked ram accelerator. This equation is used to develop the technique for high velocity operation of the ram accelerator put forth later in this thesis.

The assumptions made above were used to simplify the analytical derivation of the thrust equation. The derivation is intended to show how the thrust is affected to the first order, and will be utilized in *qualitatively* determining the best approach to demonstrating high velocity operation. When calculating the actual thrust acting on the ram accelerator projectile, a computer code is used[14] in which enthalpies $h_1$ and $h_2$ are determined as a

function of temperature, based on tabulated data. Note, as well, that Eqn. 2.16 determines the thrust acting on a projectile at a given point. To determine the thrust at any point in the ram accelerator tube, the equation must be iteratively solved, taking changes in Mach number into account. As the Mach number increases, the corresponding total enthalpy increases, resulting in an increase in static temperature at the choke point which decreases the amount of heat released, $Q$, due to dissociation losses.[14] This reduction in $Q$ causes a reduction in thrust. However, the reduction is very slight. A much more significant first-order effect is the reduction in thrust due to increasing $M_1$. In theory, as the projectile accelerates, the thrust will drop to zero when the projectile is traveling at the Chapman-Jouguet detonation velocity, $V_{CJ}$.

## 2.2 Computer Code

The computer code used in this work is a derivative of the SUPL code written by Knowlen, based on routines originally developed by Bruckner. The code iteratively solves the conservation equations, determining the enthalpies $h_1$ and $h_2$ as a function of temperature based on tabulated data. The code is initiated by computing the chemical equilibria of the combustion products for an assumed pressure and temperature. The equilibria are determined via a model given by Strehlow,[14] based on 13 reactive molecules: $O_2$, O, $H_2$, H, OH, $H_2O$, $CH_4$, CO, $CO_2$, $N_2$, N, NO, $NO_2$; plus an inert specie. Heat release is determined by the predicted combustion products, which allows the total enthalpy of the flow leaving the control volume to be calculated and compared to the total enthalpy entering the control volume. Since the total enthalpies must be equal, the static temperature is iteratively modified to raise or lower the total enthalpy of the exiting flow as needed, and the pressure is updated based on the equations of state and conservation of mass. The thrust is then determined from the conservation of momentum.

## 2.3 Comparison to Experiment

Experiments have shown that this one-dimensional blackbox theory matches quite well with experimental data. Figure 2.2.a shows this comparison, plotting velocity vs.

distance for an experiment wherein a projectile was inserted into a mixture of $2O_2 + 2.8CH_4 + 5.7N_2$ at a pressure of 25 bar. The solid line indicates the theoretical performance and the triangles indicate the experimental performance. The Chapman-Jouguet detonation speed, $V_{CJ}$, for this mixture is 1686 m/s; at this speed there is theoretically no thrust on the projectile. At approximately 1500 m/s, or 89% $V_{CJ}$, the projectile begins to deviate from the theory as it accelerates through the transdetonative velocity range and into the superdetonative propulsive mode, attaining a speed of approximately 116% $V_{CJ}$. Figure 2.2.b shows the nondimensional thrust plotted against the Mach number; again, fairly good agreement with theory up to transdetonative velocities is observed.

## 2.4 Geometry Independence

The theory developed here only takes into account the flow entering and exiting the control volume; nowhere does the theory consider the geometry of the projectile. The flow is assumed to be supersonic upon entry to the control volume and sonic upon exit. To meet these assumptions, the nose of the projectile must accept the flow and diffuse it, and the projectile body must stabilize a shock wave on or behind it such that combustion leading to thermal choking is achieved. These are the only criteria for the flow inside the control volume. Thus the blackbox theory cannot predict whether the inlet conditions will actually allow ram acceleration to occur.

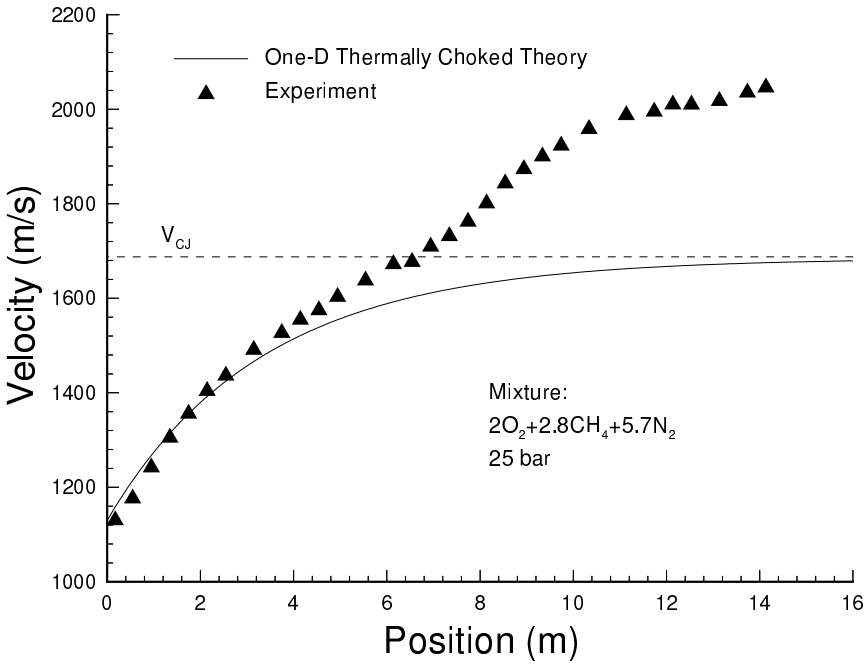


**Figure 2.2.a: Comparison of experiment to one-dimensional blackbox theory in velocity vs. position.**

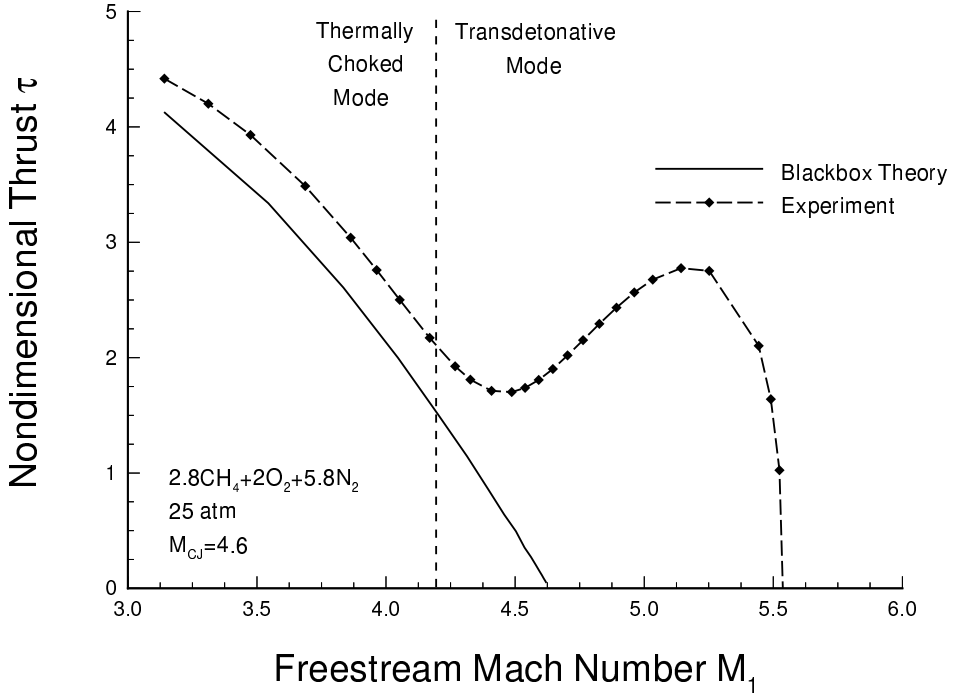


**Figure 2.2.b: Comparison of experiment to one-dimensional blackbox theory in nondimensional thrust vs. Mach number.**

# 3. Theoretical Approaches to High Velocity

From Eqn. 2.16, it can be seen that for the one-dimensional, thermally choked theory, the thrust, $\tau$, acting on a ram accelerator projectile varies only with $M_1$, $\gamma$ and $Q$, or, put mathematically, $\tau = \tau(M_1, \gamma, Q)$. The latter two terms are physical characteristics of the propellant mixture. The first term, $M_1$, varies with the speed of the projectile and the nature of the propellant mixture.

The ultimate application of the research presented is not to obtain higher thrust, per se, but to obtain higher velocities. With that in mind, Newton's second law can be applied to the thermally choked one-dimensional equation for thrust, which gets "redimensionalized" by $p_1 A$, to produce:

$$a = \frac{F}{m} = \frac{\tau p_1 A}{m} = \frac{p_1 A}{m}\left(M_1\sqrt{\frac{2}{(\gamma+1)}\left(1+\frac{\gamma-1}{2}M_1^2+Q\right)}-(1+M_1^2\gamma)\right) \qquad (3.1)$$

This is the equation for the acceleration acting on a ram accelerator projectile. The equation provides the theoretical basis for the approach to high velocity operation presented in this work.

Clearly, to increase the velocities obtainable in the thermally choked ram accelerator, it is necessary to increase the acceleration. From Eqn. 3.1, there are several ways to do that. Before continuing, however, it can be shown that the thrust, and hence acceleration, does not vary much over a wide range of values of $\gamma$. Figure 3.1 shows $\tau$ plotted against $\gamma$ at $M_1 = 3.0$, for different values of $Q$, and clearly shows a virtual lack of dependence on $\gamma$. For the propellant mixtures used in the research presented here, mixtures of oxygen and methane diluted with helium, $\gamma = 1.45 \pm 0.1$.

Looking at Eqn. 3.1, there are five remaining ways to increase the acceleration acting on a thermally choked ram accelerator projectile:

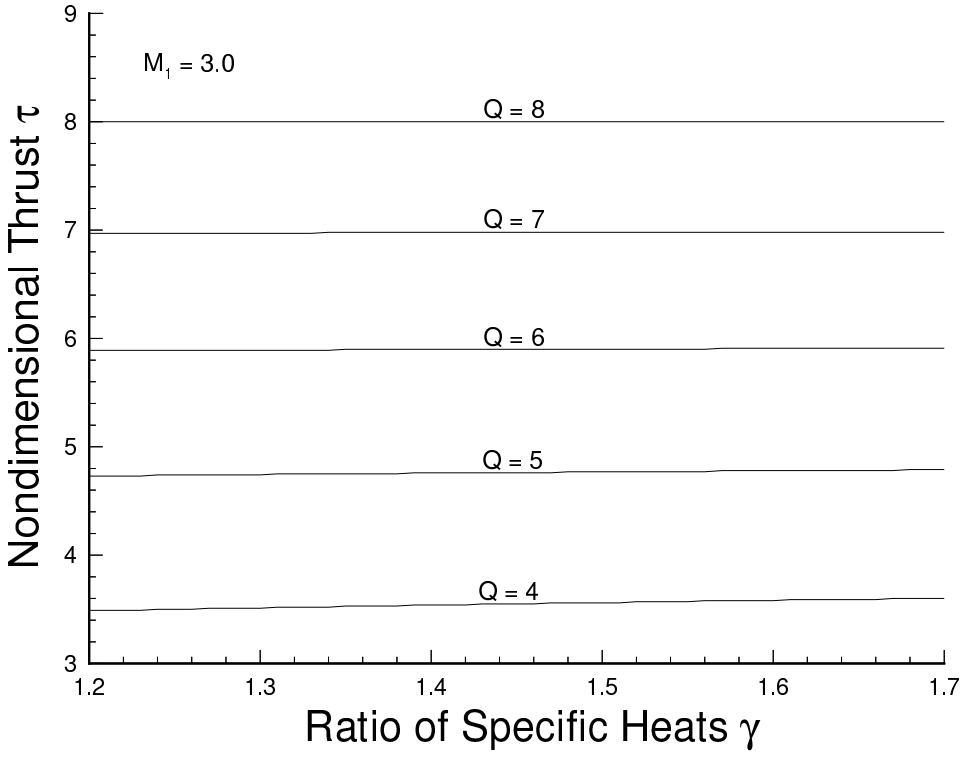


**Figure 3.1: Nondimensional thrust vs. the ratio of specific heats for various values of nondimensional heat release.**

- Increase $p_1$, the pressure of the gaseous propellant mixture through which the projectile travels
- Increase $A$, the cross-sectional area of the flow
- Decrease $m$, the mass of the projectile
- Increase $Q$, the nondimensionalized heat release of the gaseous propellant mixture
- Change $M_1$, the Mach number of the projectile

In this chapter, each of these methods is examined.

## 3.1 Increase Fill Pressure

From Eqn. 3.1, the acceleration acting on the ram accelerator projectile is directly proportional to $p_1$, the pressure of the gaseous propellant mixture, also referred to as the

fill pressure. Fill pressure limitations are primarily issues of hardware: the tubes through which the projectile travels must be able to withstand the very high pressures produced by the shock waves attached to the projectile as it travels down the tube; these shock pressures can range up to 20 times the fill pressure. In addition, there are instances when an overdriven detonation wave moves over the nose of the projectile, resulting in pressure increases of up to 50 times the fill pressure.[15] The ram accelerator hardware must be able to withstand such high pressures.

At very high pressures, one-dimensional thermally choked theory underpredicts performance. This is due to the assumption that the reacted gases obey the ideal gas equation of state, which neglects intermolecular interactions and is introduces errors for flow above approximately 10 bar. To correct this problem, it is possible to incorporate a compressibility factor, which shifts the chemical equilibria of the reactions. Figure 3.2, taken from Reference 16, shows the effect of taking compressibility into account in the thermally choked one-dimensional theory. At 50 bar, the calculated nondimensional thrust increases by 9% over thrust calculated assuming an ideal gas.

## 3.2 Increase Tube Cross-sectional Area

Increasing the tube diameter would lead to an increase in area that the exiting flow pushes against, resulting in more thrust. However, the area of the ram accelerator tube is closely coupled with the projectile mass. Increasing the area without altering the size of the projectile would change the dynamics of the flow such that the flow might not achieve subsonic conditions behind the throat, and thermal choking. If the projectile *shape* were to remain the same, but the size were to increase with the increase in tube cross-sectional area, a *decrease* in acceleration would occur because the mass would increase at a rate faster than the cross-sectional area due to the square-cube law.

For example, say that the length of the projectile is to be doubled, and it is manufactured as a shell such that 3% of the projectile volume, $V$, is mass of density, $\rho$. The mass of the projectile is then $m_1 = 0.03V\rho$. If the tube radius, $r$, were doubled, the

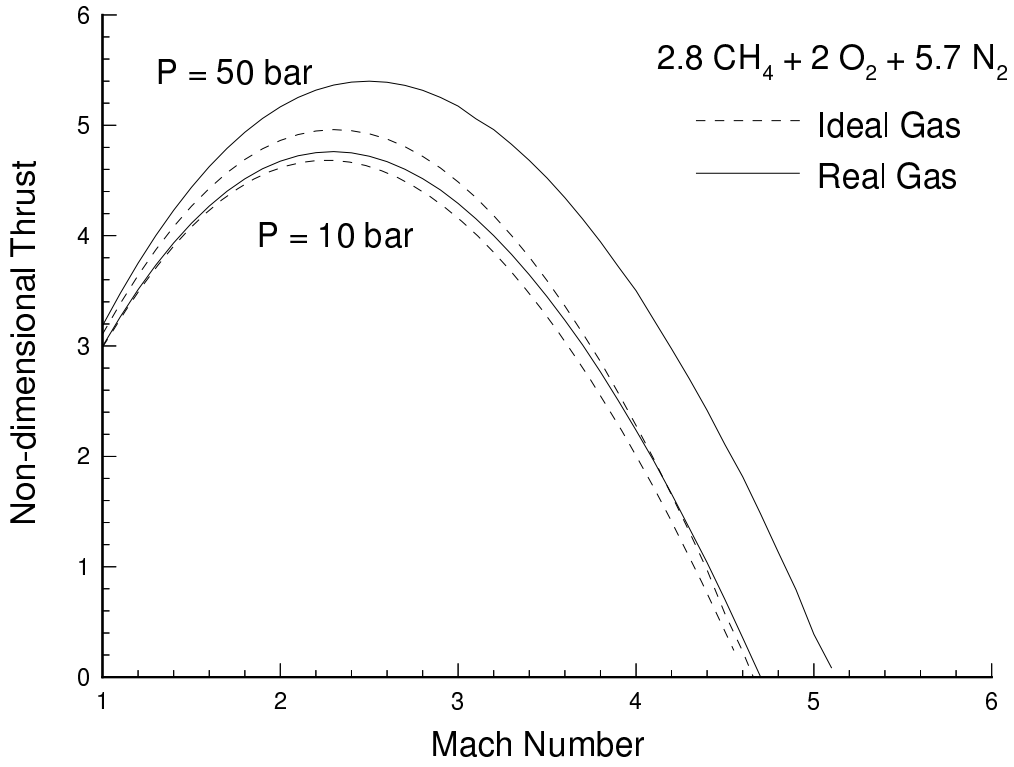


**Figure 3.2: Nondimensional thrust vs. Mach number, taking compressibility effects into account (from Reference 16).**

cross-sectional area would increase from $A$ to $4A$. Assuming the length of projectile must also double to maintain the shape, the projectile volume would increase from $V$ to $8V$. If the same criterion is applied such that the projectile is a shell that is 3% mass of density $\rho$, and taking the density to be the same, $m_2 = .03*8V\rho$, or $8m_1$. So even though the cross-sectional area has increased by a factor of four, the mass has increased by a factor of eight, leading to a *decrease* in acceleration by a factor of one-half.

## 3.3 Decrease Projectile Mass

As just described, the mass, $m$, of the projectile can be closely coupled to the cross-sectional area. If the cross-sectional area is taken to be fixed, the acceleration is inversely proportional to the mass. As stated in the previous chapter, the one-dimensional thermally choked theory utilized here only requires that the flow be rendered subsonic

behind the projectile. The simple geometry depicted in Fig. 3.3 can achieve this.

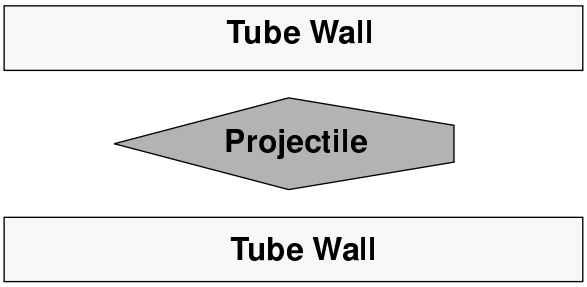


**Figure 3.3: Simple projectile geometry.**

Realistically speaking, however, there are several other factors which affect the projectile geometry. The projectile must be able to operate over a range of Mach numbers, which affects the location of the conical and normal shocks on the body. This places certain requirements on the size of the projectile nose, body, and throat, that is, the point of minimum flow area between the projectile and tube wall. In addition, the projectile needs to be stabilized as it travels down the tube. Two methods are currently in use, either equipping the projectile with fins which contact the tube wall (as is done at the UW facility), or equipping the tube wall with rails,[8] allowing the projectile to remain subcaliber (Fig 3.4). The thickness, number and shape of the fins or rails can have some affect on performance. All of these geometry parameters can effect the overall mass of the projectile. Reducing projectile mass will be discussed in greater detail in Chapter 6.

## 3.4 Increase Heat Release

Looking at Eqn. 3.1, the acceleration acting on the ram accelerator projectile varies with the square root of $Q$. This is graphically illustrated in Fig. 3.5, which shows $\tau$ plotted against $M_1$ for increasing values of $Q$ with $\gamma = 1.45$. Operating in mixtures with high amounts of heat release has been the subject of a great deal of experimental research on ram accelerators. While the thermally choked, one dimensional theory accurately predicts performance, as shown in Fig. 1.3, it does not predict what types of propellant mixtures and associated values of $Q$ will support ram accelerator operation. That it, the theory

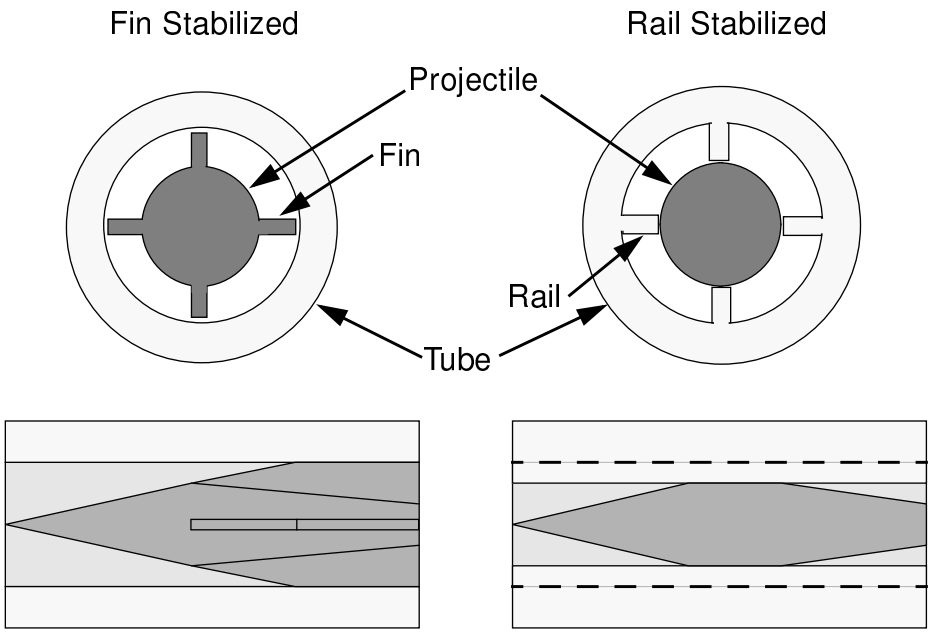


**Figure 3.4: Comparison of fin stabilized and rail stabilized projectile/wall configurations.**

predicts *how* the projectile will work, but not *if* it will. If a mixture cannot sustain ram acceleration, what often happens is that the projectile experiences an "unstart." As stated above, it is possible for an overdriven detonation or shock waves to be forced over the nose of the projectile. This is a consequence of an unstart (sometimes called more specifically a gasdynamic or wave unstart), and causes an immediate cessation in thrust, since the pressure wave is no longer pushing the projectile but rather is travelling down the ram accelerator tube ahead of it. The significant pressure increase behind the wave often causes structural damage and/or complete destruction of the projectile. Alternatively, failures could be caused by structural collapse associated with the operating conditions of ram acceleration, and not by a wave being disgorged over the projectile nose. In either case, a cessation of thrust occurs.

Higgins, et al. investigated the range of gasdynamic unstarts and concluded that the range of values of $Q$ which support ram acceleration is highly dependent upon the specific mixture used.[13,17] They observed that for a mixture of methane and oxygen at a

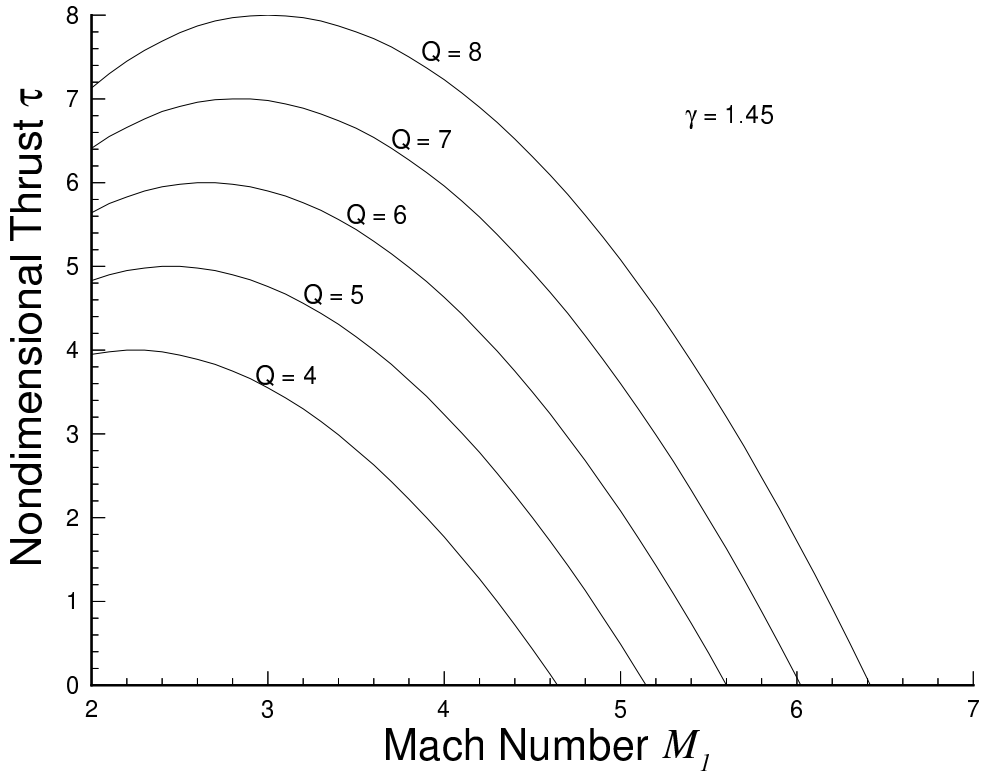


**Figure 3.5: Nondimensional thrust vs. entry Mach number for increasing values of *Q*.**

fuel equivalence ratio* of 2.8 diluted with nitrogen, the highest $Q$ which would successfully drive a projectile through the thermally choked regime was $Q \sim 5.5$.[17] For a mixture of hydrogen and oxygen with a fuel equivalence ratio of 0.5 diluted with methane, the highest amount of heat release was $Q \sim 5.5$.[13] For mixtures of stoichiometric methane and oxygen diluted with carbon dioxide, heat release values on the order of $Q \sim 8.5$ have been observed to successfully drive a projectile.

Clearly, while increasing $Q$ is key to obtaining higher acceleration levels, the specific propellant mixture must be carefully considered. Furthermore, the mixture not

* The fuel equivalence ratio is defined to be the number of moles of methane relative to the number required for a stoichiometric mixture. For an oxygen/methane mixture, $2O_2 + CH_4$ is stoichiometric, so the fuel equivalence ratio in this case is the number of moles of $CH_4$.

only affects the heat release, but also affects the sound speed of the mixture and hence the Mach number of the flow over the projectile, $M_1$. This is the subject of the next section.

## 3.5 Change Entry Mach Number

Referring to Fig. 3.5, there exists a maximum value of $M_1$ for a given $Q$, i.e., a given propellant mixture. However, the nature of the projectile geometry is such that the flow must remain supersonic over the projectile throat. Below a certain Mach number, the flow will choke on the projectile nose, immediately decelerating the projectile. This Mach number is referred to as the "diffuser unstart" limit.[18] Isentropic flow relations can easily yield a theoretical value to this limit based solely on the ratio of the throat area to the tube area and on $\gamma$, which is a function of the propellant mixture. A typical value for the isentropic diffuser unstart limit is $M_{in} \sim 2.5 \pm 0.4$. However, the limit has been experimentally observed to be slightly higher, probably due to viscous effects and shock waves.

From Fig. 3.5, it can be seen that the isentropic diffuser unstart limit near the maximum thrust level for most of the values of $Q$ under consideration. Almost all ram accelerator projectiles start on the right side of the thrust curve, at a higher Mach number than that required for peak thrust. As the Mach number increases, the thrust eventually goes to zero at a Mach number equivalent to the Chapman-Jouguet detonation velocity[1] (this can be shown from a variety of theoretical approaches). In order to maintain high-thrust conditions, it is desirable to operate as close to the peak of the thrust curves as possible. This is the motivation behind *staging*.

### 3.5.1 Staging

In this method, the projectile transits from one mixture into another that has a higher sound speed. A thin diaphragm is usually used to separate the mixtures. For example, say a projectile is travelling 1500 m/s through a mixture which has a sound speed of 300 m/s, for a Mach number of $M_1 = 5$. The projectile transits into a new mixture with the same amount of heat release but with a sound speed of 500 m/s, so the projectile

is now travelling at $M_1 = 3$, moving it to the left on the thrust curve and into a region of higher thrust. Staging is widely applied to ram accelerators.

Figure 3.6 shows data from a four-stage ram accelerator experiment, wherein a projectile was accelerated through four different propellant mixtures, each with a sound speed higher than the previous stage. Figure 3.6.a plots the velocity vs. distance, and good agreement with theory is observed. In addition, from the slope of the curves, it can be observed that the acceleration in each stage is dropping as the projectile Mach number increases. Transiting into the next stage decreases the Mach number and increases the thrust, as can be observed by the increased slope of the performance curve. This can also be seen by looking at the plot of nondimensional thrust vs. distance (Fig. 3.6.b). Note that the thrust actually *increases* at the beginning of each stage. This is *not* due to thermal choking effects on thrust, however; looking at the theoretical performance data for each stage, it can be seen that the projectile enters the stage to the right of the peak in thrust. Rather, the increase in thrust at the beginning of the stages in Fig. 3.6.b is an experimental artifact due to transitional effects between the stages or, in the case of the first stage, a transient due to the initial starting process. After the transients, it can be seen that in multi-stage experiments, the performance follows the general trend of the one-dimensional thermally choked theory.

In the sample shown in Fig. 3.6, the stage lengths were chosen based on hardware limitations of the experimental ram accelerator facility. At the UW, the hardware exists for only four stages, each of which must be at least 2 m long. Previous experiments have demonstrated that the highest levels of thrust are obtainable earlier in the tube; as the projectile transits to later stages, less thrust (and hence a lower acceleration level) is obtainable. This is similar to the effect of higher thrust at lower Mach number and, indeed, the second-order relationship of acceleration to position: the most velocity gain is obtained in the beginning of the tube. A shorter stage yields a much higher gain in velocity when the velocities are lower, for a fixed amount of acceleration. For this reason, in the experiment shown, the first stage was the shortest, with the stages increasing in length down the length of the ram accelerator.

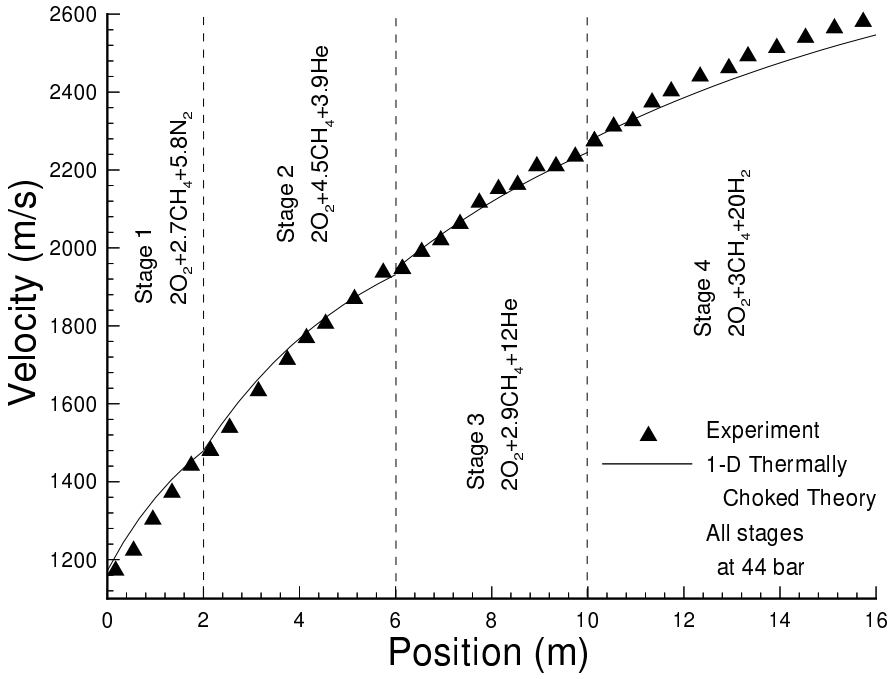


**Figure 3.6.a: Velocity vs. position for a multi-stage experiment.**

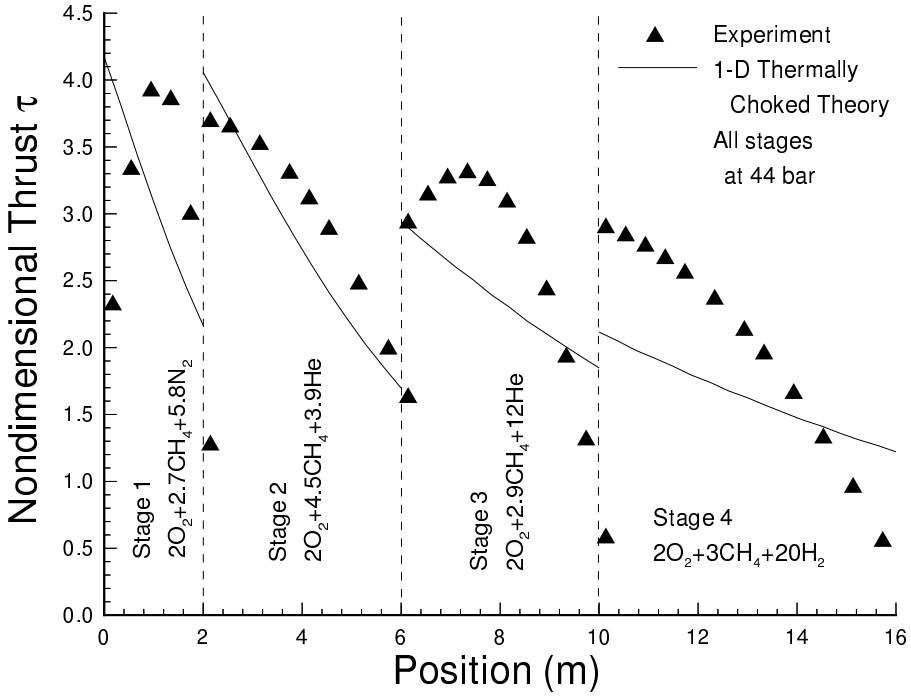


**Figure 3.6.b: Nondimensional thrust vs. position for a multi-stage experiment.**

A twist on the staging technique would be to make the sound speed of the propellant mixture increase gradually and smoothly down the tube. This could be done by using an increasing gradient of diluent from the entrance to the end of the tube. However, the practical problem of filling the graded mixture into the tube and keeping it stable until the projectile is accelerated through it confines this concept to academic idealization.

## 3.6 Increase Entrance Velocity

A final method to obtain higher velocities in the ram accelerator is to increase the velocity at which the projectile enters the ram accelerator. This approach is completely dependent on the type of prelauncher used and is independent of any aspect of ram accelerator theory or technology. Currently, all ram accelerator experimental facilities use either a conventional powder gun or a gas gun to accelerate the projectile from rest up to the entrance velocity. In all these technologies, the velocity is inversely proportional to the mass of the projectile.[19] Thus, decreasing the mass of the projectile, already identified above as an advantage in obtaining higher levels of acceleration, serves the added benefit of increasing the entrance velocity. However, for a given mixture an increase in entrance velocity will increase the entrance Mach number $M_1$. Hence, a higher entrance velocity can only be used to advantage if the propellant mixture is adjusted to maintain a low entrance Mach number.

# 4. Experimental Approach to High Velocity

Up to this point, the discussion of methods to obtain high velocities has avoided going into detail about specific ram accelerator facilities. The research effort described in this thesis was carried out at the University of Washington. It is the goal of the author that this approach to high velocities can be applied to any ram accelerator operating in the thermally choked propulsive mode. In this chapter, a general experimental approach, not specific to any facility, is described.

Referring back to the beginning of Section 3, there are five ways to increase the acceleration acting on a thermally choked ram accelerator projectile:

- Increase $p_1$, the pressure of the gaseous propellant mixture through which the projectile travels
- Increase $A$, the cross-sectional area of the flow
- Decrease $m$, the mass of the projectile
- Increase $Q$, the nondimensionalized heat release of the gaseous propellant mixture
- Change $M_1$, the Mach number of the projectile

The first two methods are limited by the hardware of the specific facility, as described in the previous chapter. The third method, decreasing the mass, $m$, of the projectile, if often limited by one or more constraints pertaining to the nature and cost of projectile manufacture.

## 4.1 Experimental Reduction of Projectile Mass

Section 3.3 described the theoretical requirements on the shape of the ram accelerator projectile. Optimally, a projectile design should be found which allows the projectile to drive through the range of subdetonative operation for the mixtures desired

and has the lowest mass possible. Realistically, that is often not possible. Cost considerations can limit the choice of materials and the extent to which the mass can be optimized. At the Mach numbers and velocities encountered in the subdetonative ram accelerator, heat transfer can play a role in projectile integrity. The contact of the fins with the tube walls (or, in the case of rail stabilized systems, the rails with the projectile body) can cause wear and alter the orientation of the projectile in the tube, a phenomenon known as canting. Canting can affect the structure of the attached shock system and the aerothermodynamic loading on the projectile, altering its performance. Severe canting can cause an unstart, whereas a normally oriented projectile would contain the pressure system rear of the throat. Several researchers have computationally and analytically modeled canting,[20] heat transfer and ablation,[21,22] thermal stress,[23] and nose heating.[24] Unfortunately, many of these models do not match well with experiments. Several experimental efforts have attempted to improve performance by varying materials[20,25] and by experimenting with projectile coatings.[8]

Relatively little experimental work has been undertaken to investigate geometrical effects on projectile performance. Although the thermally choked performance model does not require any information about the projectile's specific geometry to accurately predict performance, it does not describe the limits of operation. Higgins[12,13] thoroughly investigated gasdynamic limits of ram acceleration operation, both theoretically and experimentally, and showed a theoretical dependence of these limits on specific aspects of the projectile's geometry, particularly the throat. Schultz[26] experimentally investigated the effects of varying the throat area on the starting process in mixtures of methane-oxygen-carbon dioxide and methane-oxygen-argon. He found that decreasing the size of the projectile throat, which increases the size of the *flow throat,* increased the minimum Mach number required for starting, below which a diffuser unstart would occur (the nominal throat area ratio is $A_{throat}/A_{tube} = 0.42$). This is because an increased flow throat size allows less compression of the flow and is more conducive to disgorgement of the shock system. Figure 4.1, reproduced from Reference x, summarizes this result. No successful starts occurred for increased flow throats for the entrance Mach number range

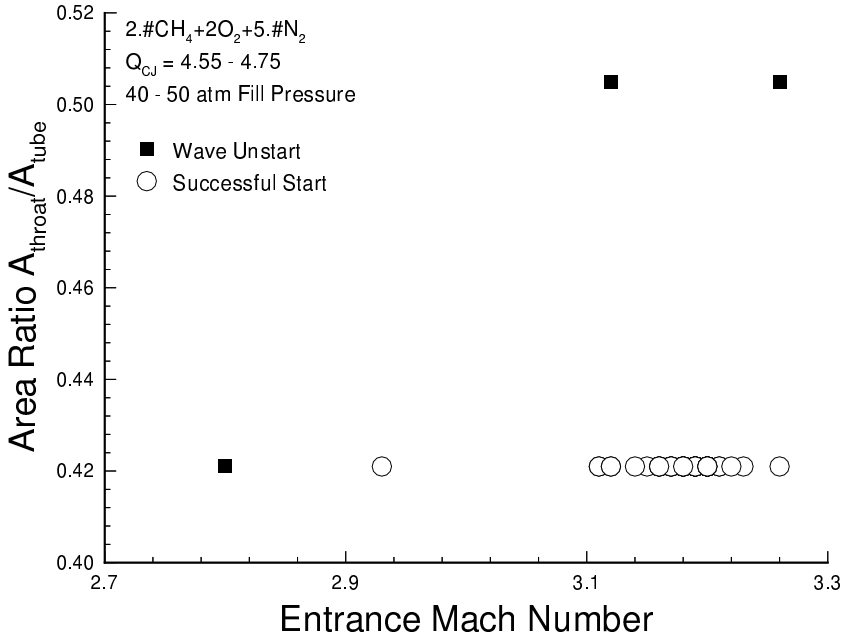


**Figure 4.1: Comparison of successful and unsuccessful shots as a function of entrance Mach number for varying flow throat areas (from Reference 26).**

under investigation, from $M_{in} = 2.8\text{-}3.3$ Imrich[18] also experimentally investigated the effects of throat area, in this case by reducing the flow throat of projectiles operating in methane-oxygen-nitrogen mixtures. He found that decreasing the flow throat area had no effect on performance except in the extreme case of reducing the flow throat area ratio to 0.25, in which case an unstart occurred immediately on entrance into the propellant mixture. Figure 4.2, reproduced from Reference 18, summarizes Imrich's throat area research. It shows that the decreased flow areas match one-dimensional thermally choked theory. Decreasing the flow throat area, however, corresponds to increasing the projectile throat diameter, which increases the overall mass of the projectile and is counter to the goals of high acceleration.

The experimental work of Shultz and Imrich described above should be applicable to other ram accelerators because the only geometric parameter varied was the area of the flow throat, one of the fundamental aspects of the ram accelerator projectile. The only

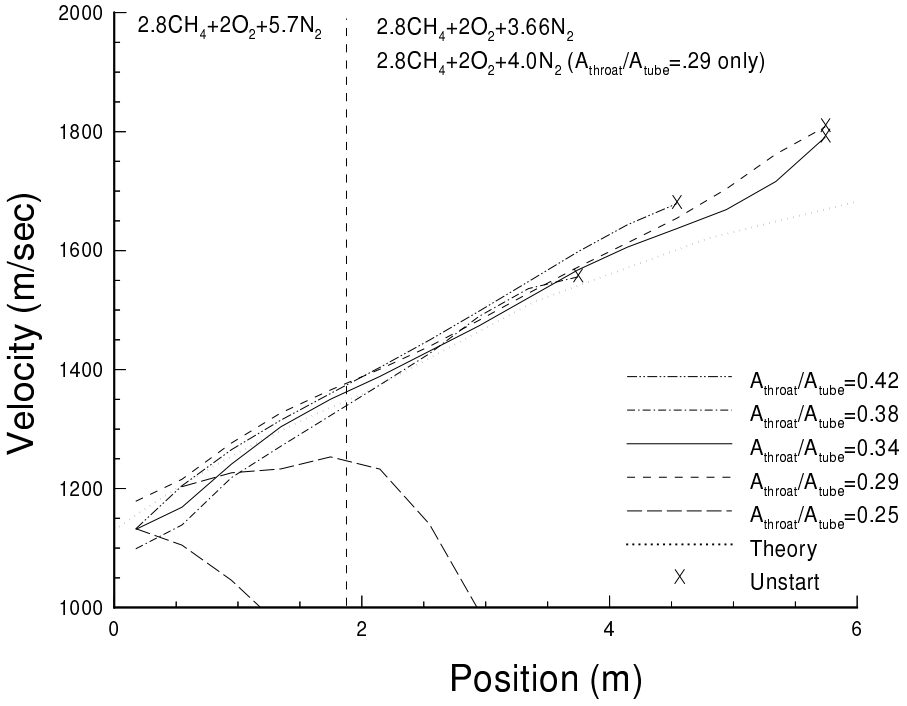


**Figure 4.2: Velocity-distance profiles for projectiles with different flow areas at the throat (from Reference 18).**

caveat is the propellant mixtures used: it has been shown that performance is very dependent on the constituents of the propellant mixture,[26] and that quantities such as the nondimensional heat release, $Q$, while effective guides to ram accelerator performance, do not wholly eliminate all the individual qualities of each propellant constituent. Fortunately, many of the various ram accelerator facilities around the world use methane-oxygen-nitrogen or methane-oxygen-carbon dioxide mixtures, as Schultz and Imrich did, so the results are likely applicable to them also.

In addition to investigating flow throat area effects, Imrich experimentally investigated the effects of several other geometric parameters in a methane-oxygen-nitrogen propellant mixture at the UW facility. These investigations are more specific to the UW facility, and will be discussed in detail in Chapter 6.

## 4.2 Mixture Maps

The remaining two approaches to increase the acceleration acting on the projectile, increasing $Q$, the heat release parameter of the mixture, and decreasing $M_1$, the entry Mach number, are both dependent on the propellant mixture used, and as such are highly coupled. To change $M_{in}$ for a fixed entrance velocity, the sound speed of the mixture must be changed, which means altering the propellant mixture, which in turn alters the heat release. Careful experimental planning is required to alter the propellant mixture such that one or both parameters are systematically varied.[27]

To better understand the relationship between $Q$ and $M_{in}$, a "mixture map" is created which shows how the two parameters vary with mixture composition. An example of such a map is shown in Fig. 4.3. Two mixture components, are plotted as the $X$ and $Y$ axes of a plane, in this case the number of moles of methane, $CH_4$ and nitrogen, $N_2$, respectively. Taking the oxidizer to be two moles of diatomic oxygen, $2O_2$, and the fill pressure of the mixture to be 50 atm, the amount of heat release is plotted as a function of the chemical composition of the mixture for a particular projectile entrance speed, 1300 m/s in the example shown (Fig 4.3.a). Regions of low $Q$ are represented by darker, bluer colors (corresponding to a "cool" mixture), while regions of high $Q$ are represented by brighter, redder colors (for a "hot" mixture). For clarity, a few lines of constant $Q$, referred to as "iso-$Q$ lines," are plotted. It can be seen that the heat release is highest at stoichiometric conditions, $2O_2 + CH_4$. Adding excess amounts of fuel or diluent reduces the heat release of the mixture.

In a given mixture, the heat release decreases slightly with increasing Mach number due to dissociation losses resulting from higher static temperatures at the plane of thermal choking.[12] Hence, the Mach number must be known to accurately calculate the value of $Q$ for a given mixture. Bearing this in mind, the sound speed can also be plotted as a function of propellant mixture. Figure 4.3.b plots lines of constant sound speed, indicating how the sound speed varies. If the entrance speed of the projectile is known, the entrance Mach number, $M_{in}$ is known as a function of the propellant composition, and

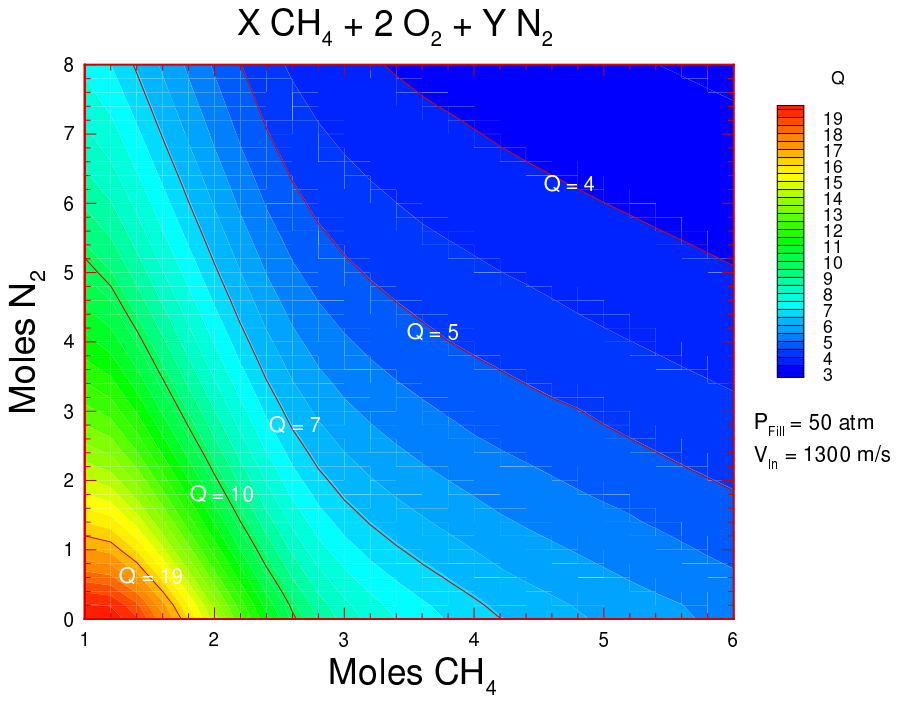


**Figure 4.3.a: Mixture map for methane/oxygen/nitrogen propellant mixtures.**

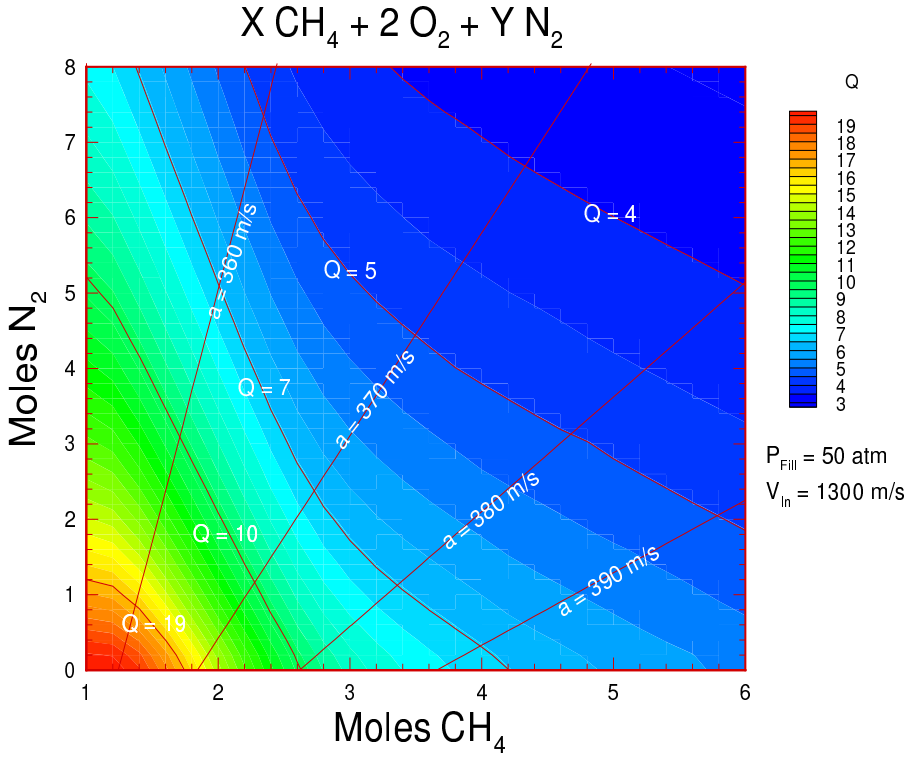


**Figure 4.3.b: Mixture map for methane/oxygen/nitrogen propellant mixtures with lines of constant sound speed.**

allows the heat release to be accurately calculated. For the sake of clearly showing the variation in nondimensional heat release, the value of $Q$ represented is that which corresponds to the projectile's entrance speed.

Figure 4.4.a plots lines of constant entrance Mach number ("iso-$M_{in}$ lines") overlaying iso-$Q$ lines. This type of plot allows one to accurately understand how both $Q$ and $M_{in}$ vary with propellant mixture for a given projectile speed. It does not show how to obtain high levels of acceleration, but rather shows regions of propellant combinations which should produce it. As stated earlier, Higgins, et al. showed that methane/oxygen/nitrogen propellant mixtures have a $Q$ limit of ~5.5. From the mixture map, it can be seen that a variety of mixtures produce $Q$=5. Knowing that decreasing values of entrance Mach number should allow higher levels of acceleration leads one to move to the lower right on the mixture map, along the iso-$Q$ line corresponding to $Q$=5, to access those higher accelerations.

The mixture map with just $Q$ and $M_{in}$ plotted shows how these parameters vary with mixture, but it does not explicitly display which mixtures will produce higher accelerations than others. However, if some detail about the experiment is known, this information can be calculated using the computer code described in Section 2.2. The code determines the thrust acting on the projectile at a given Mach number in a given propellant mixture, based on one-dimensional thermally choked flow theory. Knowing the cross-sectional area of the tube, the tube fill pressure, and the projectile mass, the theoretical acceleration at a given point can be calculated. Knowing the length of tube through which the projectile travels, i.e., the stage length, the average theoretical acceleration can be calculated. The acceleration can be calculated for a given mass traveling through a given length of tube as a function of propellant mixture. Values of acceleration can then be plotted on the mixture map.

Figure 4.4.b shows lines of average acceleration ("iso-$g$ lines") plotted over iso-$Q$ and iso-$M_{in}$ lines on the mixture map, for a projectile massing 100 gm entering a 2 m stage at 1300 m/s. The average accelerations are described in terms of $g$'s, where one $g$ is equal

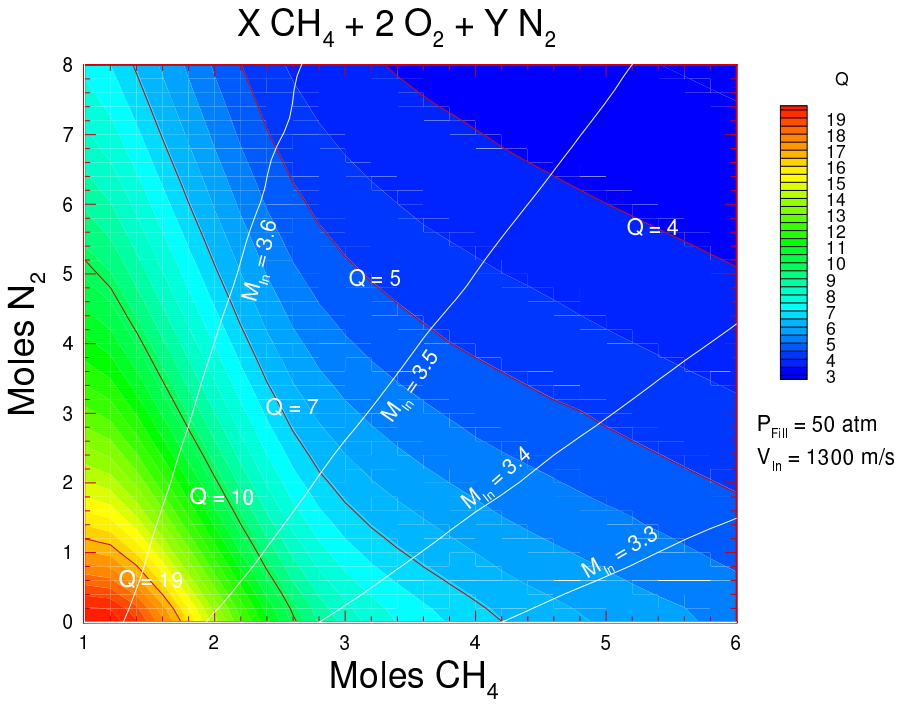


**Figure 4.4.a: Mixture map for methane/oxygen/nitrogen propellant mixtures with lines of constant entrance Mach number.**

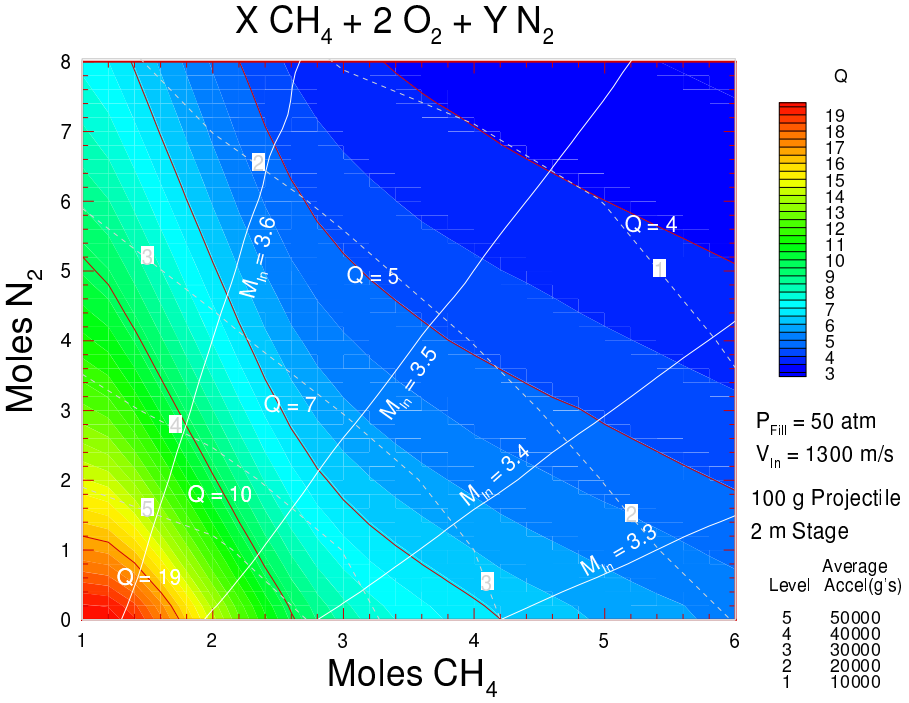


**Figure 4.4.b: Mixture map for methane/oxygen/nitrogen propellant mixtures with lines of constant entrance Mach number and constant acceleration.**

to Earth's average gravitational acceleration, 9.81 m/s.$^2$ Although this plot appears initially confusing, it is effective at discerning which mixtures will, in theory, produce high acceleration levels. The iso-$g$ lines are approximately normal to the iso-$M_{in}$ lines, but not normal to the iso-$Q$ lines, as might be expected. To attain higher accelerations, one needs to move perpendicular to the iso-$g$ lines.

Because the theory does not predict *where* on the mixture map the projectile can successfully drive, it may be necessary to do several experiments to discern whether any limits on $Q$ or $M_{in}$ exist. If they do, moving along an iso-$g$ line may still yield high performance. For example, suppose the highest permissible value of heat release is found to be $Q$~7. From Fig. 4.4.b, the $Q$=7 line is approximately parallel to the iso-$g$ line from about $M_{in}$=3.4 to $M_{in}$=3.5. So any mixture along that line should yield the highest average acceleration.

Conversely, if a limit on entrance Mach number is found, such that the projectile would not drive in any mixture with, say, $M_{in} < 3.4$, then the mixture map shows regions which should allow high performance: anywhere on the plot above and to the left of the $M_{in}$=3.4 iso-$M_{in}$ line. Experiments could then be performed to determine whether or not a limit on $Q$ exists. These experiments would then describe a region of operation on the mapping. This will be discussed further in Chapter 6.

(In reality, it is known that a $Q$ limit of $Q$~5.5 is thought to exist for the methane/ oxygen/nitrogen class of mixtures. From Fig. 4.4.b, the highest performance theoretically attainable out of this mixture is about 20,000 $g$'s.)

It is important to point out that any mixture combination that has only two variables can be described and plotted in this fashion. Nitrogen was chosen as an arbitrary diluent to describe the nature of the mixture map presented here. Such a plot could just as easily have been developed with carbon dioxide, argon, helium, etc. Methane was chosen because it is the most common fuel used in ram accelerators, but hydrogen, ethylene or a variety of other fuels could have been used as well. Indeed, it is possible to produce a plot

with four constituents, three of which are varied, by adding the third dimension to the mixture map (making it a mixture topography, rather than a mixture map). However, such a representation would be fairly difficult to comprehend, with iso-$Q$, iso-$M_{in}$, and iso-$g$ lines transformed into surfaces.

The mixture map can be applied to any type or size of ram accelerator. The map quickly identifies what propellant combinations will yield high accelerations. Several mixture maps using different diluents appear in Appendix A. With a relatively small number of experiments to determine where bounds of operation exist, near-optimal acceleration levels for a given projectile mass at a given entrance velocity can be determined. In Chapter 6, this idea is experimentally demonstrated in two stages of the UW ram accelerator.

# 5. University of Washington Ram Accelerator Facility

The ram accelerator at the University of Washington (UW) has been operational since 1985. A schematic of the facility is shown in Fig. 5.1. It is divided into three sections: the prelauncher, the ram accelerator test section, and the decelerator section. The prelauncher consists is a helium gas gun having a plenum chamber that is 102 mm diameter x 1.83 m long and capable of being loaded to approximately 375 atm, two 38.1 mm bore x 2.44 m launch tubes and an evacuated dump tank through which a 38.1 mm bore x 1.52 m vent tube passes before connection to the ram accelerator section. Blocks of solid aluminum are often used to reduce the volume in the gun's plenum to lower helium consumption. The vent tube is perforated with 36 holes of 17.1 mm diameter to vent the helium from the ram accelerator process.

The ram accelerator section consists of eight tubes, each 1.998 m x 38.1 mm bore, for a total length of 15.984 m. The tubes are connected with threaded collars and are machined such that up to about 4 mm of Mylar diaphragms can be placed between the tubes to contain the propellant mixtures and allow staging. Each tube is perforated with

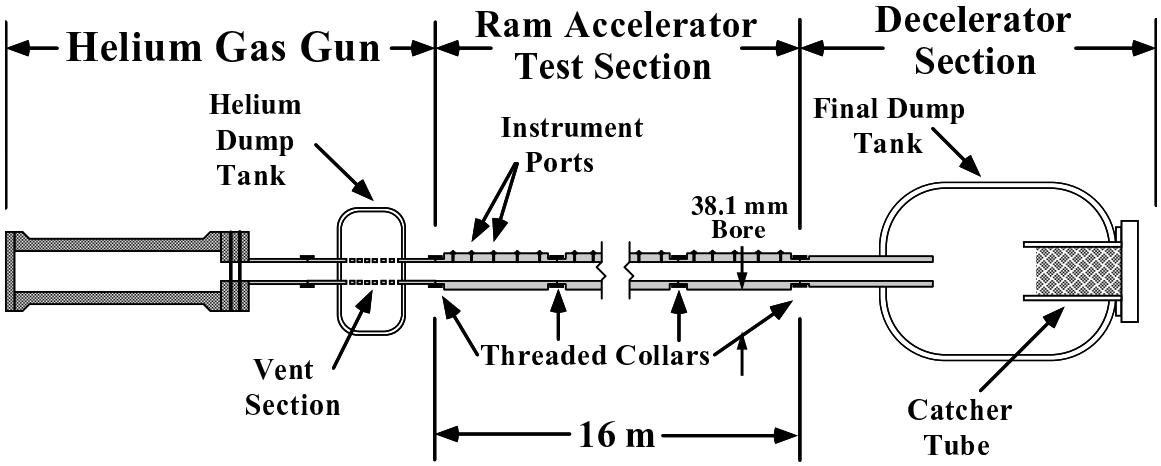


**Figure 5.1: University of Washington 38.1 mm ram accelerator facility.**

holes at five instrument stations located 40 cm apart and 19.9 cm from the tube ends. The first, middle and last instrument stations in each tube have four instrument ports equally spaced at 90º intervals around the circumference of the tube, while the second and fourth instrument stations have three instrument stations equally spaced at 120º intervals.

The decelerator section consists of a X cm long drift tube that connects the last ram accelerator tube with the final dump tank which is approximately 2 m long x 1.5 m in diameter. An 18 cm diameter catcher tube is located in the last 1 m of this dump tank. The catcher tube is tightly packed with plates of metal and fibrous material to destructively decelerate the projectile: impact with the metal breaks the projectile into small pieces which can be absorbed by the fibrous material. A back plate at the rear of the dump tank can be removed for access to the catcher tube.

A typical UW projectile is shown in Fig. 5.2. Projectiles are typically manufactured from either magnesium (ZK60-AT5 alloy), aluminum (7075-T6 alloy), or titanium (6Al-4V alloy). They have been manufactured in small quantities from other materials, including lexan and graphite, and have been coated with a variety of materials, including nickel and teflon, in attempts to improve performance. Typically, projectiles are manufactured in two hollow pieces, the nose and body, which thread together at the throat. The so-called "standard" projectile consists of a conical 10º half-angle nose, 29.0 mm throat, and 71.1 mm body with a 17.8 mm diameter base, 4.5º body taper angle, and four or five fins of either 3.8 mm or 3 mm uniform thickness, respectively. The mass of the

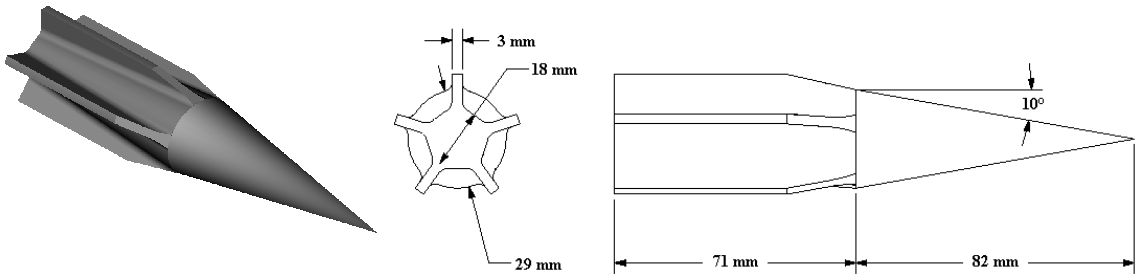


**Figure 5.2: Typical ram accelerator projectile.**

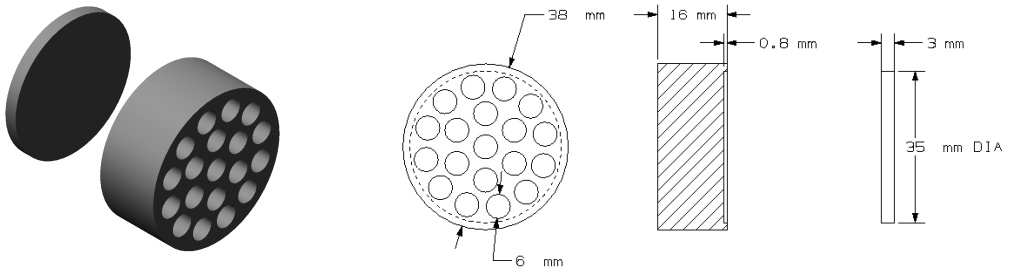


**Figure 5.3: Obturator and backplate.**

standard projectile is approximately 75 gm. However, noses have been manufactured with conical half-angles ranging from 7º to 20º, and body lengths have varied from 35 mm to 97 mm. Fin number has been varied in other studies from three to six, with thicknesses ranging from 2.8 mm to 5.1 mm.

Before the projectile is loaded into the launch tube, a full caliber obturator (Fig. 5.3) is glued to the base of the projectile. Made of a polycarbonate known by its trade name of Lexan, the obturator is perforated with 19 holes and sealed with a backplate (also made of Lexan). The purpose of the obturator is twofold: with the backplate in place, it constitutes a piston that occludes the tube and which the helium driver gas can push against (without the obturator in place, the helium would pass over the subcaliber throat of the projectile). The second purpose is to enable passive starting of the combustion process once the projectile enters the high pressure gases of the ram accelerator section.

A ram accelerator experiment (or "shot") begins by releasing the helium gas gun pressure against the sealed obturator, accelerating the obturator-projectile combination through the evacuated launch tubes and vent tube. By varying the pressure in the gas gun and the mass of the projectile-obturator combination, different entrance speeds can be attained. By the time the projectile reaches the entrance diaphragm between the vent tube and first ram accelerator tube, it can attain speeds up to 1350 m/s. The gas in the ram

accelerator tube are usually at a pressure between 25 and 50 atm. Two 0.356 mm thick Mylar diaphragms can contain the 50 atm of pressure used in high pressure experiments.

As the obturator-projectile combination pierces the diaphragm and first encounters the propellant, the backplate is blown off the back and the holes in the obturator weaken the initial shocks driven onto the projectile body by the obturator. Recent research indicates that the launch tubes are not totally evacuated, and that a series of reflected shocks through the trace amount of air between the incoming obturator-projectile and initial Mylar diaphragm raises the pressure and temperature, and is crucial to the initiation of combustion.[28] The starting process is poorly understood compared to other aspects of ram accelerator operation, but recent research by Stewart[28] and Schultz[26] has provided crucial details about its nature.

After combustion is initiated, the projectile moves through the propellant gases, accelerating to higher velocities, until it either transits into another stage, transits out of a stage into an evacuated ram accelerator tube or the drift tube, or experiences an unstart. At present, the UW facility is configured to fill up to four stages. Diaphragms can be placed between any individual tubes, allowing for stage lengths longer than 2 m.

The projectile is tracked via electromagnetic transducers located in the instrument ports which pick up the signal of a ring magnet located at the projectile throat. The electromagnetic transducers have a response time of 1 μs and are connected to a similarly fast data acquisition system which times the signals as it acquires and stores them, allowing the velocity of the projectile to be calculated from distance-vs.-time data. The instrument ports can also be equipped with either pressure or fiber-optic transducers. The fiber-optic transducers provide qualitative data based on luminosity generated during combustion. The pressure transducers use piezoresistive crystals to measure the pressure of the flowfield at the tube wall and provide quantitative data, also with a response time of 1 μs. By analyzing data from the pressure transducers, it is possible to deduce the nature of the flowfield around the projectile.

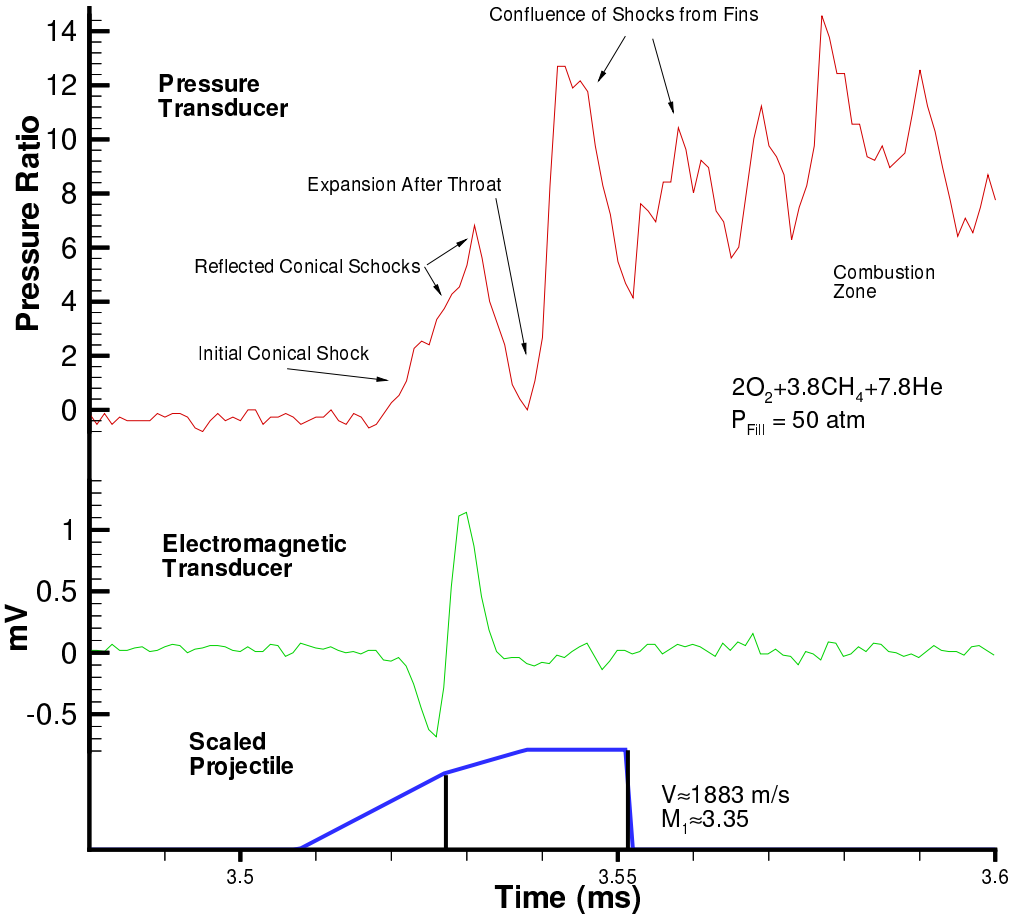


**Figure 5.4: Typical instrument data from a UW ram accelerator experiment.**

Figure 5.4 shows typical signals from the electromagnetic and pressure transducers vs. time. Knowing the dimensions of the projectile and its velocity, it is possible to display the projectile's features varying with time, as shown at the bottom of Fig. 5.4. Note that the peaks on the electromagnetic transducer trace appear at the projectile throat, the location of the magnet. The pressure transducer trace at the top of Fig. 5.4 shows the pressure rise due to the initial and reflected conical shocks, and the pressure decrease from the expansion around the throat. The normal shock wave following the throat is not a distinct standing wave, as shown in the idealized schematic in Fig. 1.1, but rather appears as a series of shock waves due to multiple reflections from the projectile fins.

# 6. Experiments and Results

With the methods to attain high velocity identified, they were systematically applied to the UW ram accelerator.

## 6.1 Increase Fill Pressure

The fill pressure of the UW ram accelerator is limited to 50 atm by both the tube material and the hardware used to inject the propellant mixture into the tube.

## 6.2 Increase Cross-Sectional Area

The cross-sectional area of the UW ram accelerator is fixed at 11.40 cm.$^2$

## 6.3 Decrease mass

In addition to investigating the effects of projectile throat area on ram accelerator performance, Imrich experimentally investigated the effects of varying the nose cone half-angle, body length, fin thickness, and number of fins on subdetonative performance.[18] His goal in this effort was to find a low mass projectile design that would match the performance of the standard projectile (Fig. 5.2) up to the transdetonative operating mode. The results are summarized below. All experiments were performed using aluminum projectiles into a propellant mixture of $2.8CH_4 + 2O_2 + 5.7N_2$, except where noted. The fill pressures used in the experiments varied; the plotted results identify the pressures used.

### 6.3.1 Nose Angle Variations

Imrich varied the nose conical half-angle from 7º to 20º in approximately 2.5º increments, using a nominal 71 mm body. The results appear in Fig. 6.1. Only the 20º and 17.5º noses failed to drive to velocities greater than $V_{CJ}$. From the results, it appears that the lowest mass nose for successful subdetonative performance has a 15º conical half-angle.

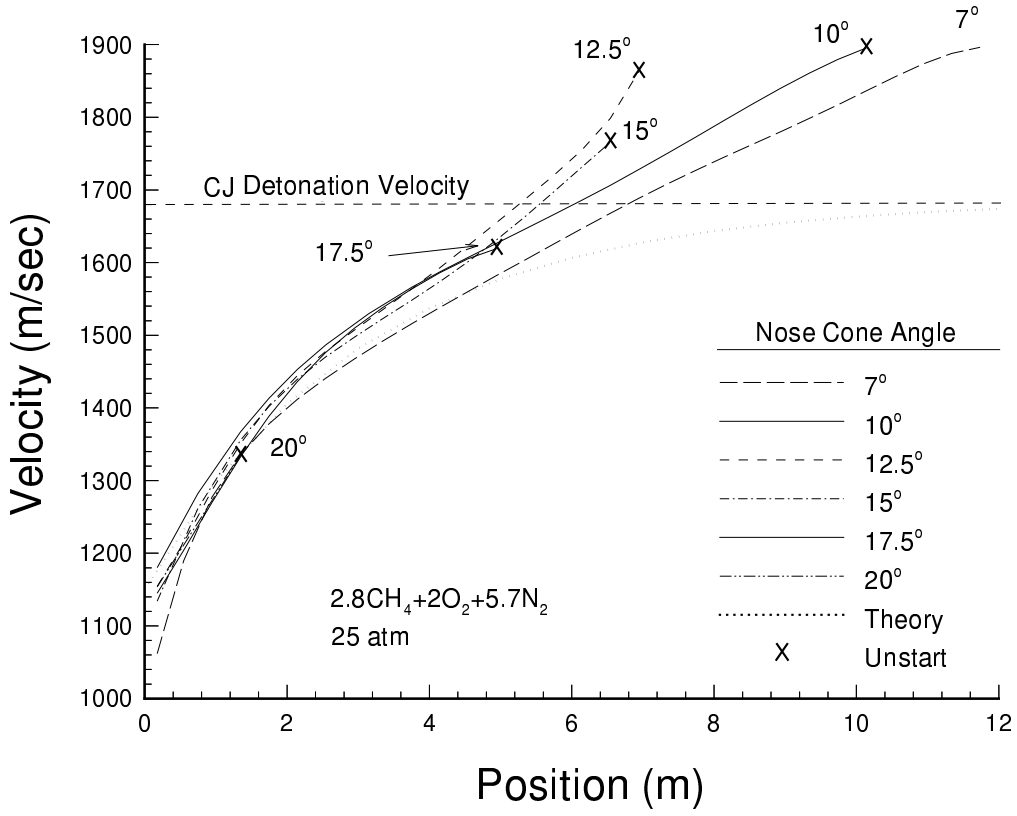


**Figure 6.1: Velocity vs. position for nose conical half-angle variations with 71 mm body.**

### 6.3.2 Body Length Variations

In this series of Imrich's experiments, the body length was shortened from the nominal 71 mm to 35 mm in 9 mm increments. Two series of experiments were performed, one with a nominal nose half-angle of 10º and one with a half-angle of 15º. Figure 6.2 shows the velocity histories for these experiments, with $V_{CJ}$ as a reference. From Fig. 6.2.a, it can be seen that for the nominal nose, all but the 35 mm body drove through the subdetonative regime. Note that as the bodies were shortened, the acceleration increased due to the reduced mass. Figure 6.2.b shows that, again, only the 35 mm body failed to drive to at least $95\%V_{CJ}$. In addition, the other body lengths all unstarted at approximately the same velocity. From these data, it is evident that a

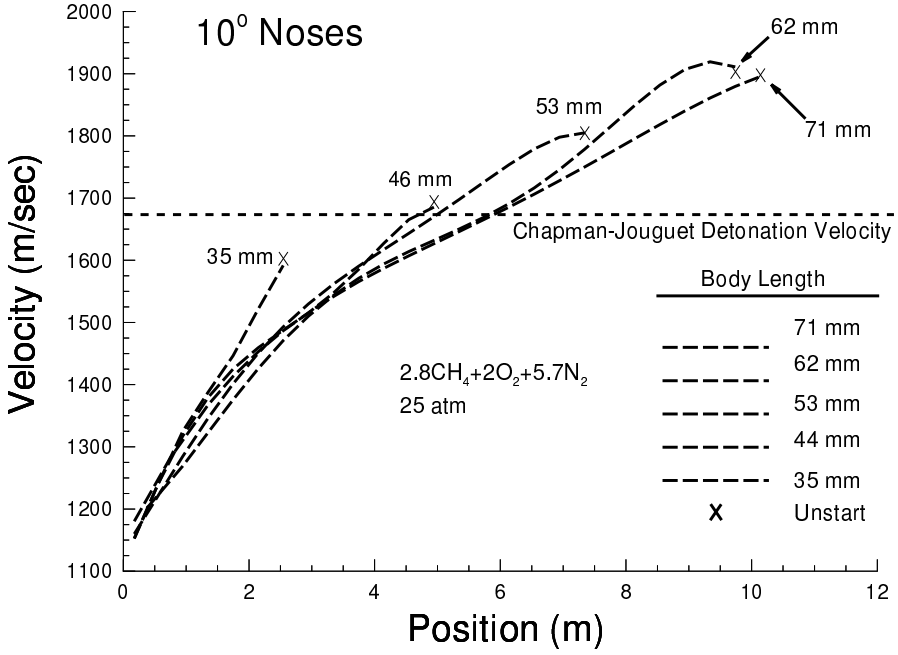


**Figure 6.2.a: Velocity vs. position for body-length variation with 10° nose.**

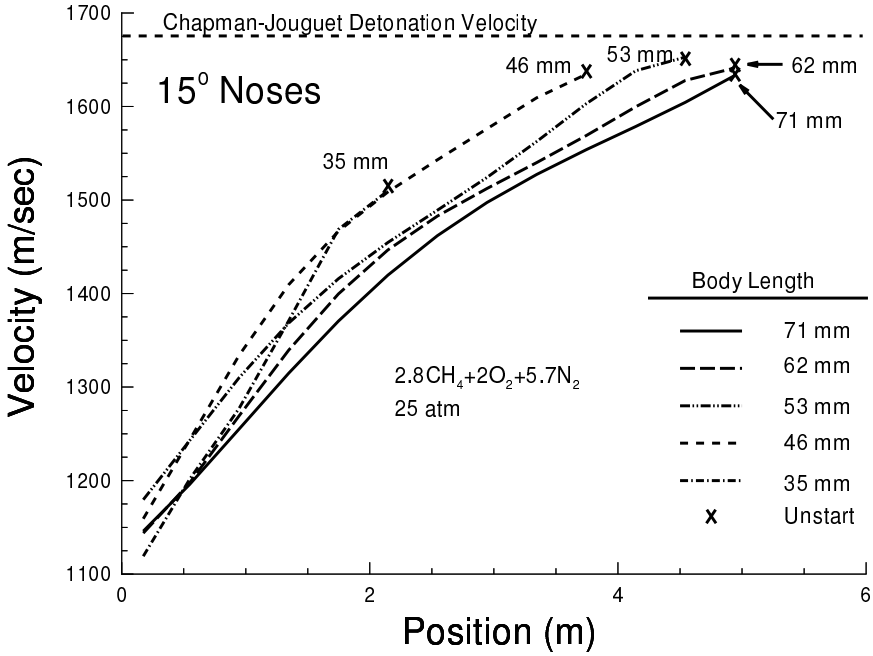


**Figure 6.2.b: Velocity vs. position for body-length variation with 15° nose.**

projectile with a 46 mm body is the shortest (and hence lowest mass) that will drive through nearly the entire subdetonative velocity regime, for either nose-cone angle.

### 6.3.3 Fin Thickness

To determine the effects of fin thickness, magnesium projectiles were manufactured in four-fin configurations with fin thicknesses varying from 2.77 to 5.13 mm, corresponding to the fin thicknesses traditionally found on 3-, 4-, 5-, and 6-finned projectiles. Magnesium was selected instead of aluminum in an effort to reduce machining costs. Figure 6.3 shows the results of this experimental series. The thickest and thinnest fin thicknesses failed to accelerate to $V_{CJ}$. Imrich concluded the failures were

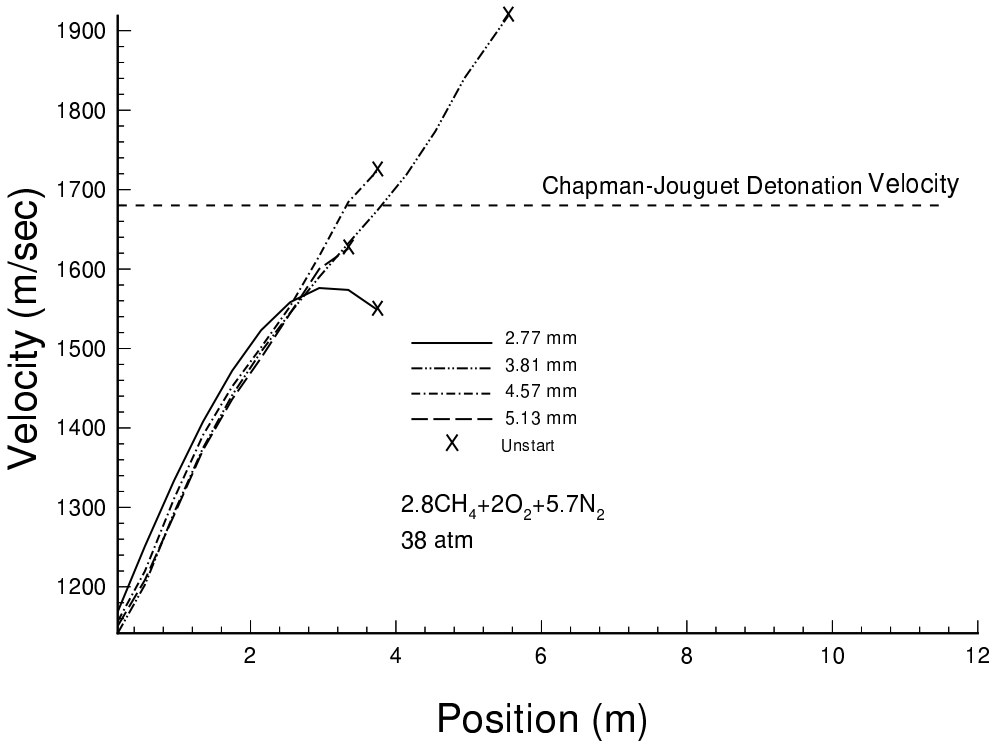


**Figure 6.3: Velocity vs. position for fin thickness variations.**

structural in nature, and that no clear increase in performance was visible with either thicker or thinner fins compared to the 155 $mm^2$ standard thickness.

### 6.3.4 Number of Fins

This experimental series by Imrich varied the number of fins from 3 to 6. The relevant results appear in velocity vs. position format in Fig. 6.4. From these data, it is

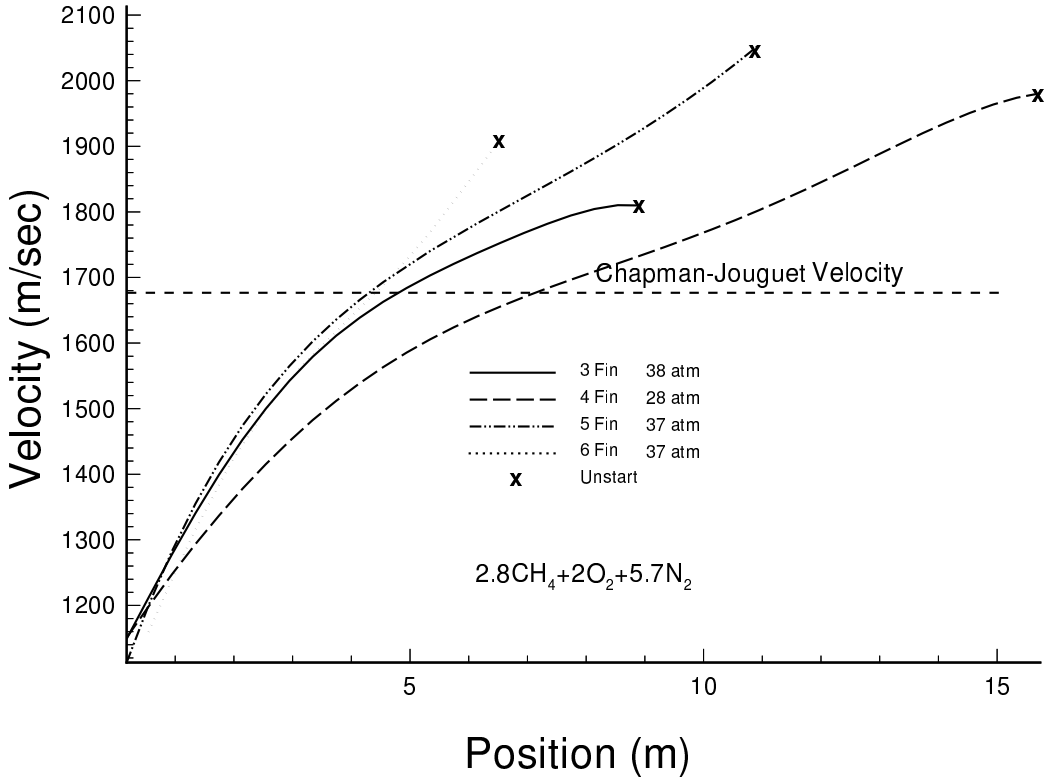


**Figure 6.4: Velocity vs. position for fin number variations.**

evident that all projectile configurations drove past $V_{CJ}$, but any further conclusions cannot be driven. The variation in accelerations is due to differing masses.

### 6.3.5 Reduced Mass Projectile

From Imrich's experiments, a projectile design was developed which has a 15º conical half-angle nose, a 46 mm body, and four fins with a thickness of 3.8 mm (Fig. 6.5).

The reduced mass projectile has a mass of approximately 50 gm when manufactured from aluminum alloy, corresponding to a reduction in mass of a third compared to the "standard" projectile. This is the projectile design used in all the high velocity experiments described here.

Note that the projectile mass has *not* been optimized. The incremental changes in the various geometric parameters were relatively coarse, and none of the experiments were repeated. Rather, the projectile mass has been *minimized* based on the available data.

## 6.4 High Velocity Experimental Series

With the results of Imrich's work applied to produce the reduced mass projectile described above, experiments were undertaken, using the mixture maps, to find near-optimal propellant mixtures for high acceleration levels. Operation in the first two stages was thoroughly experimentally explored, and preliminary experiments were performed on the third stage.

### 6.4.1 High Velocity First Stage

It was initially experimentally determined that the helium gas gun could accelerate the reduced mass projectile to an entrance velocity of $V_{in} = 1320$ m/s. A mixture of methane and oxygen with no diluent was initially used, followed by mixtures of methane, oxygen and helium. Helium was chosen as a diluent because previous experience has shown that with this combination of propellants, it yields higher thrust than either

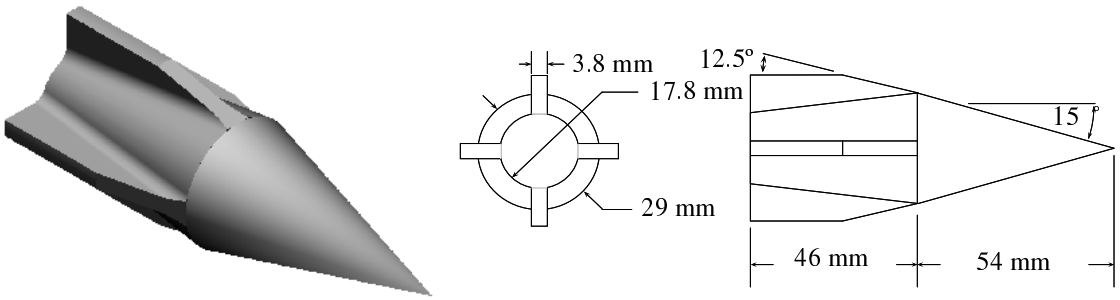


**Figure 6.5: Reduced Mass Projectile.**

nitrogen, hydrogen, or carbon dioxide, the other diluents typically used. From a theoretical standpoint, helium is well-suited to the technique presented because it is more effective at lowering the sound speed of the propellant mixture, compared to hydrogen or nitrogen.

Figure 6.6.a shows a mixture map for methane/oxygen/helium mixtures at 50 atm fill pressure. Iso-$Q$, iso-$M_{in}$ and iso-$g$ lines are plotted. The iso-$g$ lines are plotted based on a 50 gm projectile traveling through a 2 m stage which it enters at 1320 m/s. For this class of propellant mixtures, the iso-$g$ lines are nearly vertical. The amount of helium in the mixture does not significantly affect the theoretical accelerations. However, it clearly affects the iso-$M_{in}$ lines and the iso-$Q$ lines.

The first stage experiments were performed using 8 m stage lengths. The motivation for this was finding a propellant mixture which would successfully drive the projectile *slightly farther* than the 2 m stage length. Previous experience has shown that as acceleration levels are increased, unstarts occur earlier in the tube.[13] A desirable propellant mixture for the first stage is one which can reliably provide high acceleration levels without experiencing an unstart. A criterion was applied which defined a successful experiment as one which drove at least 2 m. As it turned out, all successful experiments drove at least 3 m.

The results appear on the mixture map in Fig. 6.6.b. White triangles indicate propellant mixtures wherein the projectile drove at least 3 m. Red triangles indicate mixtures where that criterion was not met. As it turns out, unstarts were observed in the first meter of all unsuccessful experiments.

Arrows on the mixture map indicate the order of the experiments. The arrows are alphabetically labelled to follow the series of experiments. Initially, only methane/oxygen mixtures were used. Upon the first successful experiment, $Q$ was increased by reducing the amount of methane in the mixture (making it less “fuel rich”), increasing performance

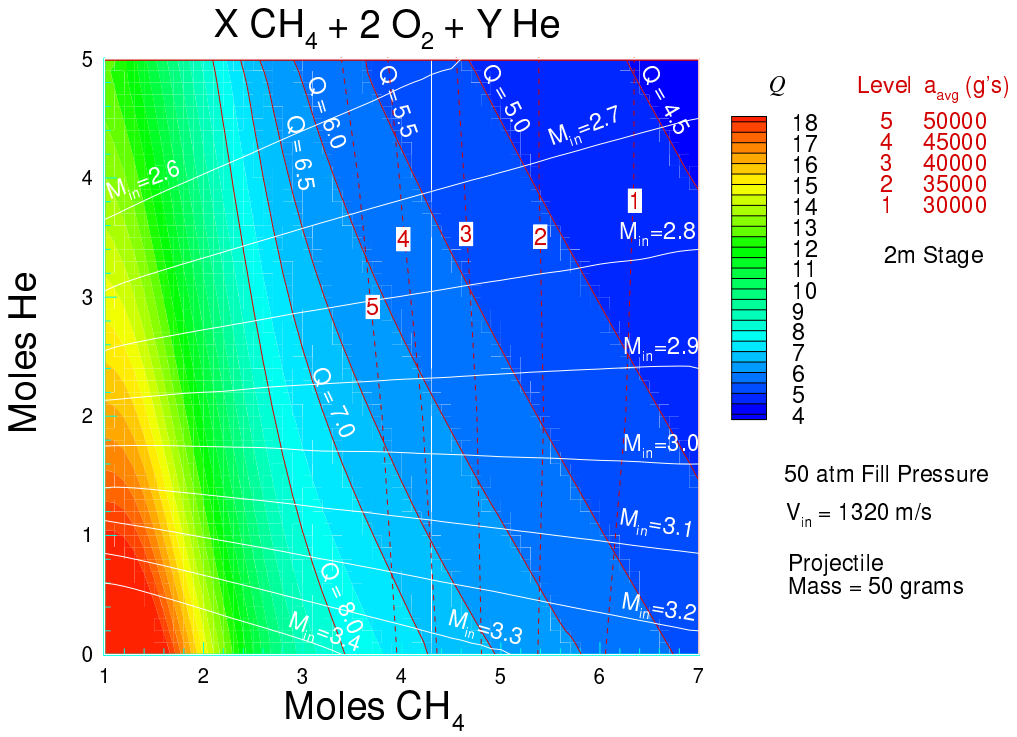


**Figure 6.6.a: Methane/oxygen/helium mixture map for the first stage.**

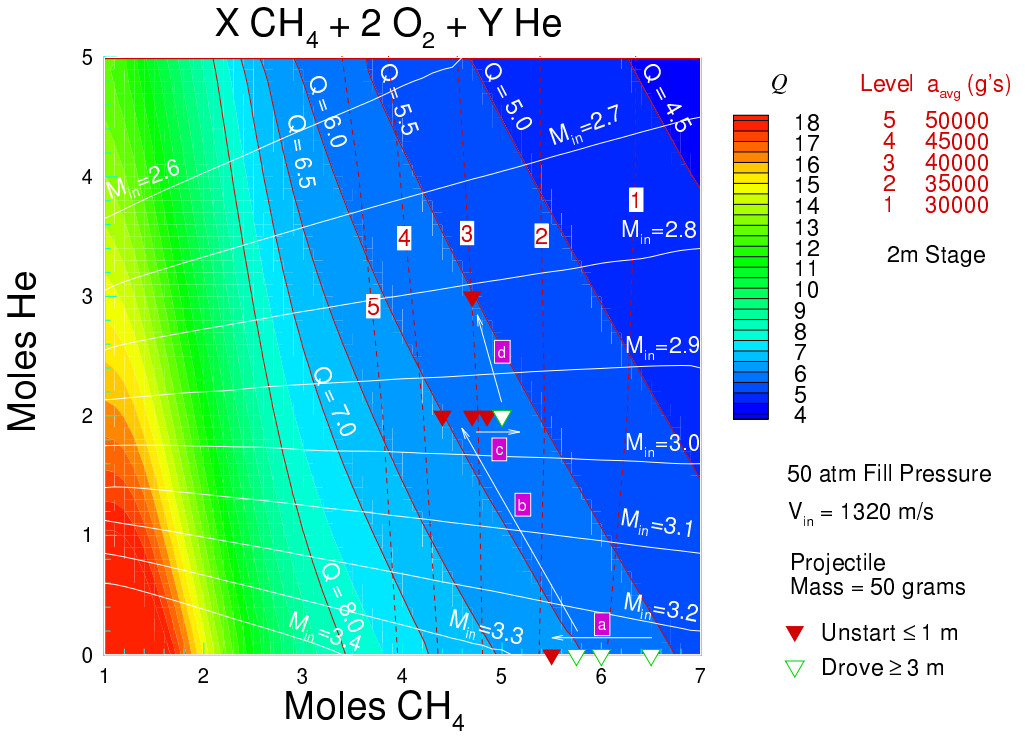


**Figure 6.6.b: Methane/oxygen/helium mixture map for the first stage with experiments shown.**

(arrow (a)). That process was repeated until an unstart was observed, in a mixture of $2O_2$+$5.5CH_4$.

At this point, helium was added to reduce $M_{in}$. Taking the limit at $5.5CH_4$ to be related to $Q$, the next propellant mixture used the highest $Q$ from the successful experiments, $Q = 6.0$, with helium added to reduce the entrance Mach number, $M_{in}$ (arrow (b)). Two moles of helium were added, for an entrance Mach number of $M_{in} = 2.95$. Note that in adding the helium to reduce $M_{in}$ while staying on the same iso-$Q$ line, iso-$g$ lines are crossed, allowing higher acceleration levels to be realized. Put another way, moving along the iso-$Q$ line moves to the left of the iso-$g$ lines, so higher acceleration should occur. In this experiment, an unstart occurred. Again believing a $Q$-limit to exist, methane was varied to reduce $Q$ until a successful shot was observed (arrow (c)). This mixture, $5CH_4$+$2O_2$ + 2He, although at a lower $Q$ ($Q = 5.7$) than the highest performing methane/oxygen mixture, actually produces a higher acceleration due to the effect of reduced $M_{in}$.

The same process was repeated in an attempt to obtain even higher acceleration. The entrance Mach number was reduced while keeping $Q$ constant (arrow (d)). Note that a slightly cooler $Q$ was used. The motivation for this was that in the step from methane/oxygen to methane/oxygen/helium mixtures, $Q$ had to be reduced to find a propellant mixture which would successfully drive the experiment. As such, the trend was followed and $Q$ was reduced slightly, from $Q = 5.7$ to $Q = 5.6$. Note that the reduction in $M_{in}$ was not as great as the previous step, because the diffuser unstart limit was approached. The resulting mixture was $4.7CH_4$+$2O_2$+3He. An unstart was observed in this propellant mixture. Reducing the $Q$ as before would not have been of any advantage, however, because it would reduce the acceleration level to that of the successful experiment in the $5CH_4$+$2O_2$+2He mixture. The latter is the mixture found to be the highest performing first stage experiment, and was used as the first stage in subsequent stage development.

The results of the successful first stage experiments appear in velocity-position format in Fig. 6.7. More detailed information appears in Appendix B. Three experiments

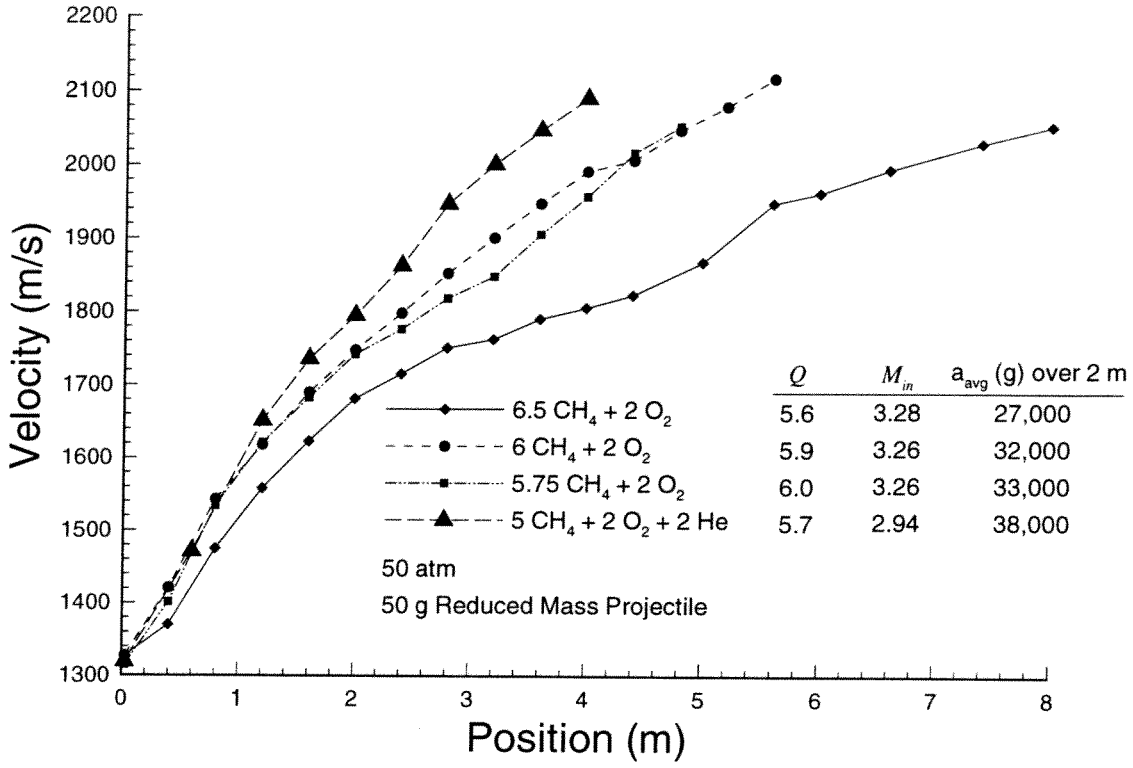


**Figure 6.7: Successful first stage high velocity experiments.**

with just methane and oxygen were performed, as can be seen in the summarized data on the plot. Unstarts were observed in all propellant mixtures except the methane/oxygen mixture with the lowest $Q$, $6.5CH_4 + 2O_2$. As the amount of methane was reduced, $Q$ increased, increasing the observed average acceleration. Note that $M_{in}$ for these mixtures was approximately constant. As described above, when helium was added, the highest performing propellant mixture was one with a lower $Q$. However, the helium reduced $M_{in}$, allowing higher average acceleration to be observed. This acceleration, 38,000 *g's*, is one of the highest ever recorded at the UW facility over a 2 m stage length. Note, as well, that as the acceleration increased with varying mixtures, the unstarts occurred earlier in the tube.

Finally, it should be pointed out that the performance was maximized within the resolution of the variation used in the propellant chemistry. Just as with Imrich's

experiments,[18] the mixture has *not* been optimized, but rather the highest performance has been found within the resolution of the increments in chemistry used.

### 6.4.2 High Velocity Second Stage

The first stage development using the mixture maps demonstrated that a mixture of $5CH_4+2O_2+2He$ could accelerate a 50 gm projectile from $V_{in}$ ~ 1320 m/s to $V$ ~ 1800 m/s in 2 m. Using 1800 m/s as the entrance velocity, a mixture map for the second stage was generated, again using methane as the fuel and helium as the diluent (Fig. 6.8.a.).

Comparing the mixture map for the second stage to that for the first, it can be seen that iso-$Q$ lines are less vertical and the iso-$M_{in}$ lines less horizontal. The reason for this is that the resolution of the $X$- and $Y$-axes has been changed from the first stage map to the second. In order to keep the sound speed high enough to keep $M_{in}$ low at the higher entrance velocity, the mixture must contain more helium than in the first stage; with all this extra diluent, the methane/oxygen ratio must be reduced to keep the heat release, $Q$, at reasonably high levels. As such, the molar range of methane is reduced while the molar range of helium is increased to display propellant mixtures with the desired range of $Q$ and $M_{in}$.

The same technique of using 8-m stages was used, determining the propellant mixture that provided the best performance over the first 2 m. The results appear in the mixture map in Fig. 6.8.b. More detailed information appears in Appendix C. As before, white triangles refer to propellant mixtures which successfully drove at least 2 m, whereas red triangles indicated mixtures wherein an unstart occurred less than 2 m into the tube. A new symbol is introduced as well, a red circle, which refers to an experiment wherein a "wave fall-off" was observed. In this situation, the combustion behind the projectile does not release enough heat to sustain a pressure rise which matches the increase from the normal shock on the body. The flow does not thermally choke, and the pressure wave falls off the body, resulting in a cessation of thrust.

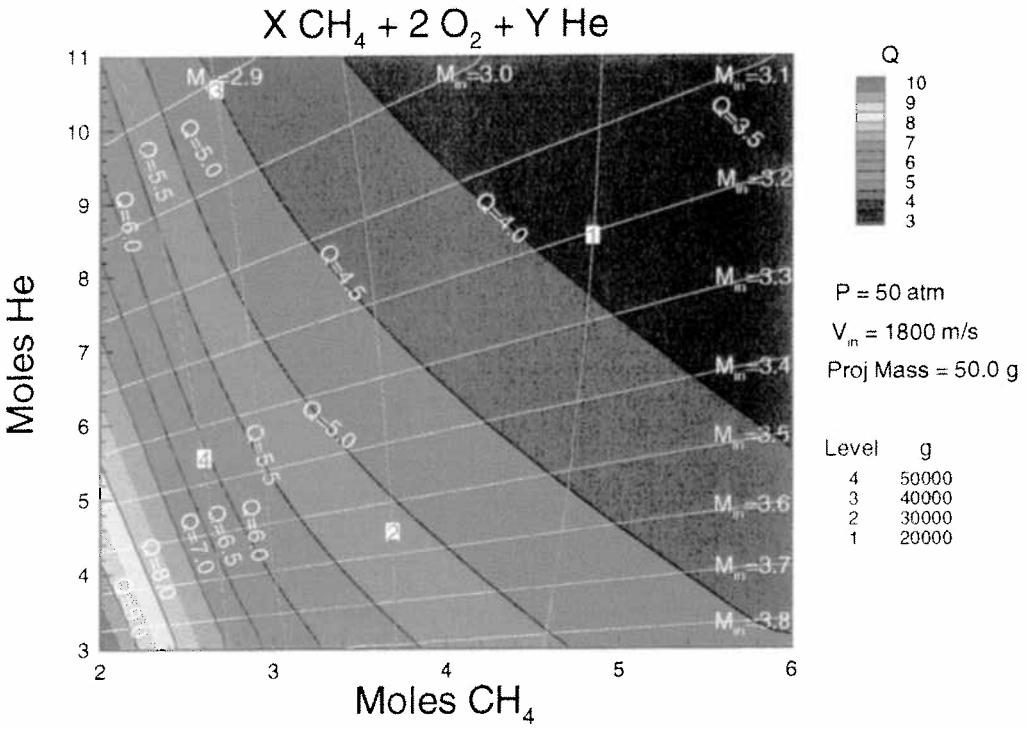


**Figure 6.8.a: Methane/oxygen/helium mixture map for the second stage.**

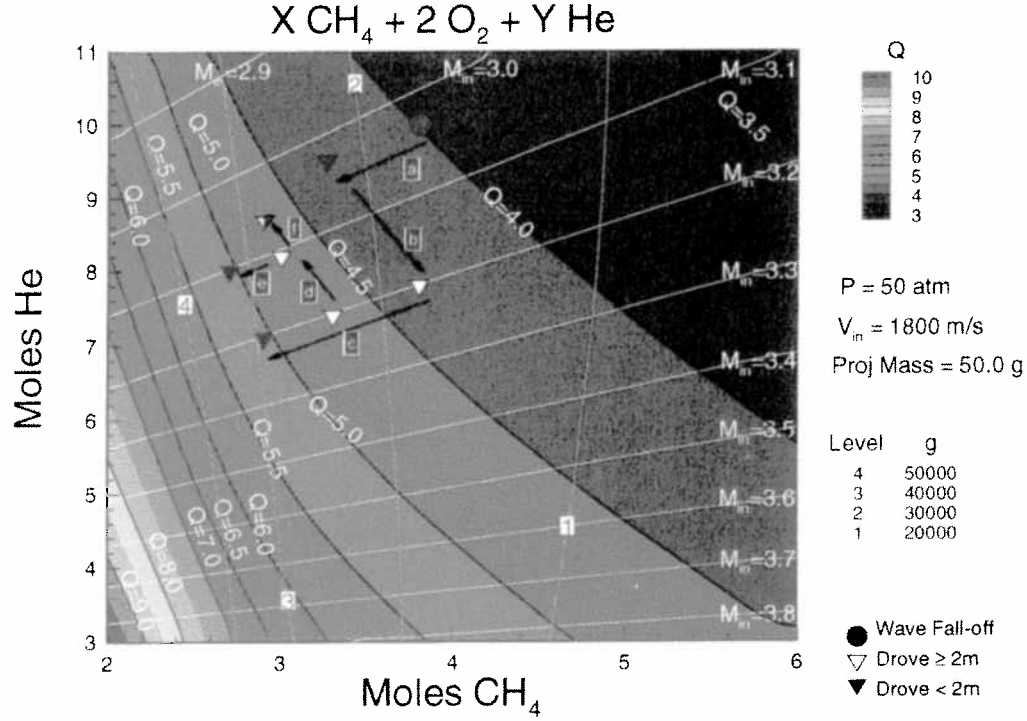


**Figure 6.8.b: Methane/oxygen/helium mixture map for the second stage with experiments shown.**

Arrows have again been added to the mixture map (Fig. 6.8.b), alphabetically labelled to follow the sequence of experiments. The first propellant mixture was selected with a cool $Q$ and moderate $M_{in}$ because of a desire to get a starting point that would work. Since any $Q$ or $M_{in}$ limits were unknown, the mixture was chosen conservatively in the hope that it would fall in a successful region; attempts at higher acceleration would be based off this initial second stage experiment. As it turned out, the mixture was too cool to support ram acceleration: the wave fall-off was observed. Heating up the mixture (arrow (a)) while staying on the same iso-$M_{in}$ line resulted in the opposite problem: a wave unstart. It was theorized that perhaps the Mach number was too low and a $M_{in}$ limit was being observed, so the entrance Mach number was increased while keeping $Q$ constant (arrow (b)).

This experiment, at $M_{in} = 3.2$, was successful, so the mixture was heated up, yielding higher acceleration levels, until a wave unstart was observed (arrow (c)). Taking the highest successful value of $Q$ along this iso-$M_{in}$ line, the entrance Mach number was then reduced to $M_{in} = 3.1$ to determine whether higher acceleration was possible, which was observed (arrow (d)). The same process was again applied: heating up the propellant mixture while keeping $M_{in}$ constant (arrow (e)), which was unsuccessful.

The last attempt at higher acceleration in this mixture followed the same idea as above, moving along the iso-$Q$ line of a successful experiment to an even lower $M_{in}$, this time splitting the difference between $M_{in} = 3.03$, which was tried at the beginning, and $M_{in} = 3.05$, which had already been tested (arrow(f)). This propellant mixture successfully drove the projectile 2 m, yielding a record 42,000 average acceleration over 2 m, but an unstart was observed *immediately* after the projectile entered the second 2 m tube. In addition, data from the pressure transducers indicated the projectile was very close to experiencing an unstart. A repeat experiment was performed into the mixture, and an unstart was observed about 1 m into the second stage. These experiments are represented by the two-colored triangle in Fig. 6.8.b.

The propellant mixture used in the successful experiment at the intersection of arrows (d), (e), and (f) is the one chosen for a second stage mixture. The experiment was successfully repeated for validity. Note that in just ten experiments, a high-performance second stage propellant mixture was found, $3CH_4 + 2O_2 + 8.2He$, that yielded average accelerations of approximately 36,000 g. A range of heat release from $Q = 4.0$ to $Q = 5.25$ was investigated, along with a range of entrance Mach number from $M_{in} = 3.03$ to $M_{in} = 3.2$. High performance was found by using the mixture maps to move perpendicular to the iso-$g$ lines. The mixture maps allow limitations on heat release and Mach number to be found quickly by judiciously selecting the experiments performed.

The successful experiments from the second stage development appear plotted as velocity vs. position in Fig. 6.9, along with a comparison of $Q$ and $M_{in}$ and the average

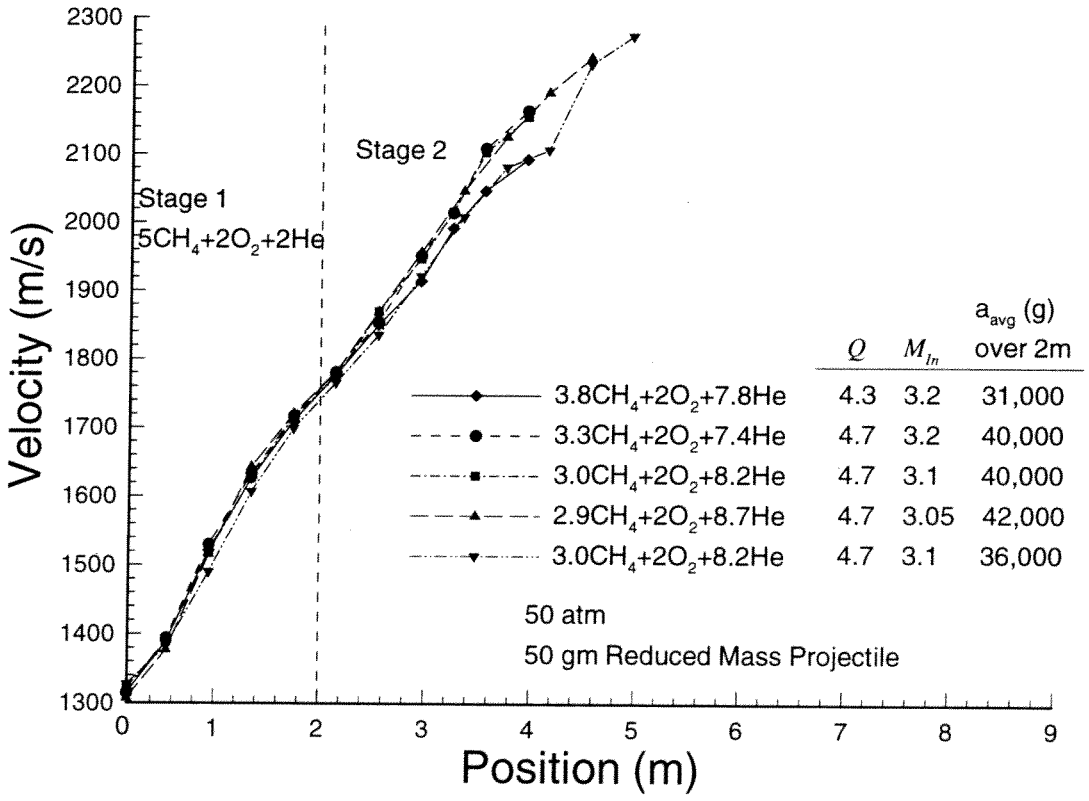


**Figure 6.9: Successful second stage high velocity experiments.**

acceleration. The fifth experiment listed is a repeat of the third. Note that although the experiments were performed using the same propellant mixtures, there is a 10% difference in average acceleration. From the mixture map in Fig. 6.8.b, the lower value matches better with theory. For many of the high velocity experiments, the projectile outperformed the theoretical acceleration. This is in part due to real gas effects described earlier. Other factors causing the increase in acceleration can be speculated upon, such as perhaps the projectile is wearing down slightly, losing mass which results in a higher acceleration. Or perhaps some of the aluminum of the projectile is reacting with the oxygen, reducing mass and increasing $Q$. These are merely speculative guesses. The true reason for the relatively large difference in acceleration between experiment and theory is unknown, and cannot be resolved without further experiments.

### 6.4.3 High Velocity Third Stage

Some preliminary work was performed to develop a high velocity third stage. Unfortunately, problems arose. It was found to be impossible to achieve successful operation of the high velocity second stage mixture, $3.0CH_4 + 2O_2 + 8.2He$, when the stage length was shortened from 8 m to 2 m. The only second stage mixture which would repeat operation in a 2 m configuration was the lowest performing mixture, $3.8CH_4 + 2O_2 + 7.8He$, with a transition velocity of $V = 2100$ m/s. This mixture was actually filled into 6 m of tube, and the last 4 m were evacuated and then filled with the third stage mixture. A third stage mixture of $2.2CH_4 + 2O_2 + 12.3He$, with $Q = 4.7$ and $M_{in} = 3.2$, was found to successfully drive a projectile over 2 m. That experiment is shown in Fig. 6.10. The experiment. however, could not be repeated.

The reasons for the failure of 2 m mixtures to operate compared to 8 m mixtures are not totally understood at this time. It was speculated that the failure is due to problems in the filling system which arise when filling different volumes.

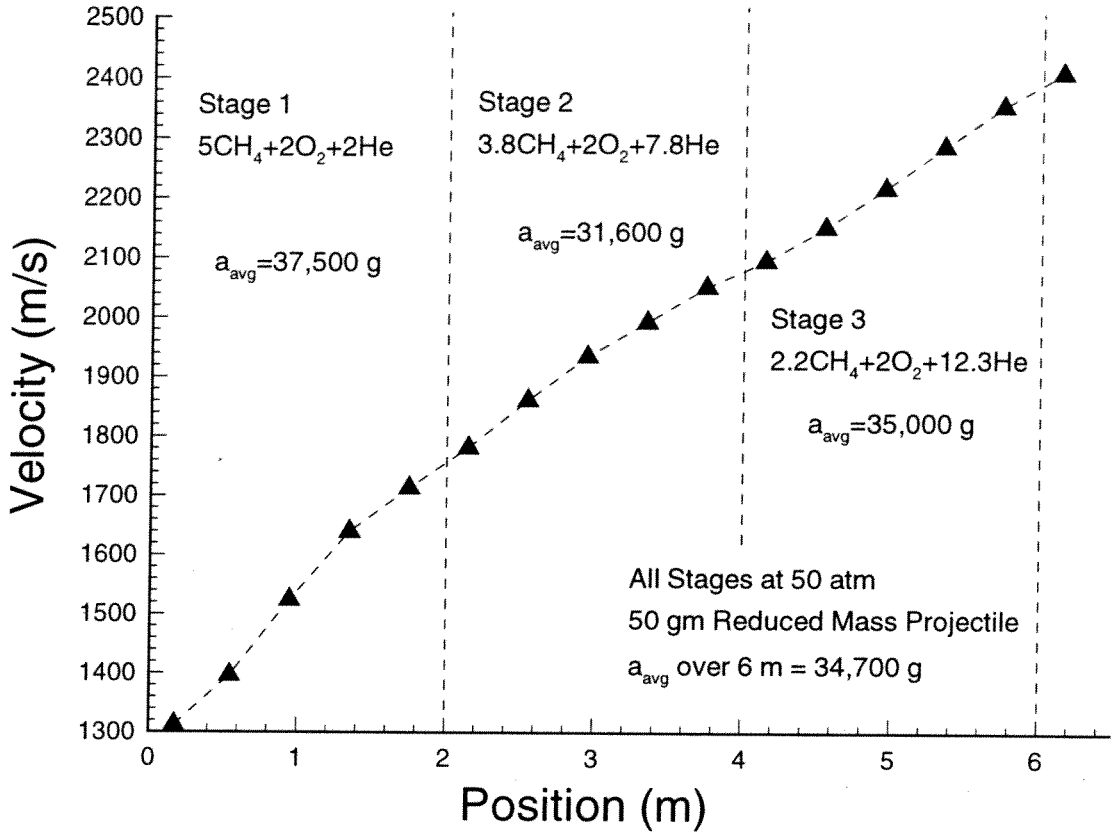


**Figure 6.10: Successful third stage high velocity experiment.**

## 6.5 High Velocity Results

The highest velocity observed in a ram accelerator (2670 m/s) occurred in late 1991 at the UW facility. Figure 6.11 plots velocity vs. performance for this experiment. The projectile masses approximately 78 gm, and was accelerated through four stages of increasing sound speed and *decreasing* $Q$, and hence decreasing theoretical average acceleration. It was found that repeatable operation was only possible after reducing $Q$ as the projectile moved from stage to stage.

Figure 6.12 compares the current effort to the record experiment. The first stage mixture of $5CH_4 + 2O_2 + 2He$ has been observed to be a repeatable mixture. However, as

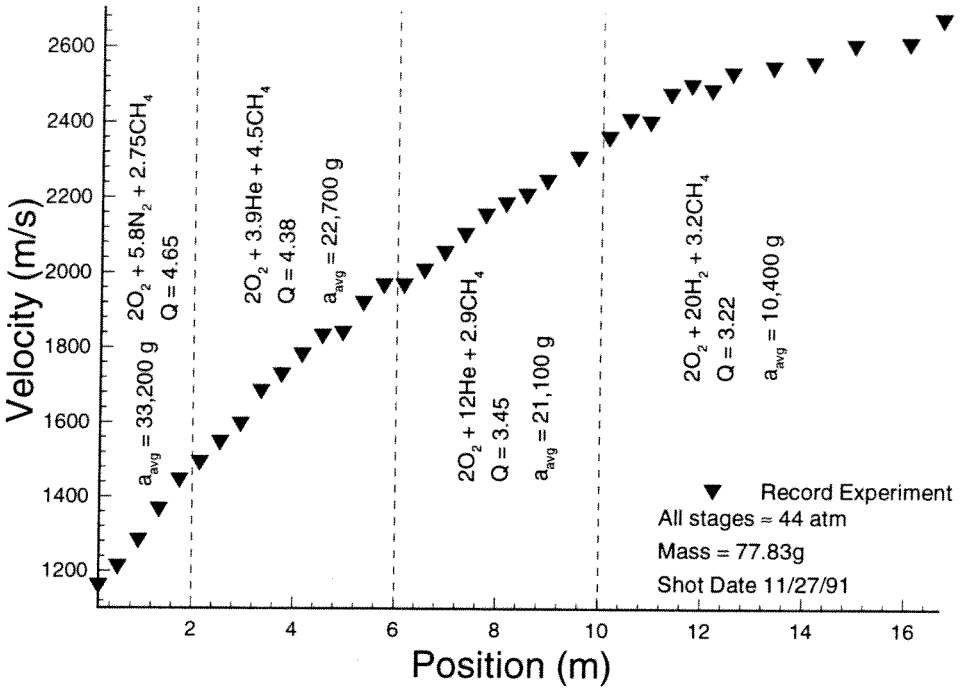


**Figure 6.11: Record velocity ram accelerator experiment (1991).**

described above, propellant mixtures that demonstrated high performance over the first 2 m in 8-m stages were not observed to successfully drive a projectile when the stage length was shortened to 2 m. In addition, the high performance in the third stage, shown in Fig. 6.10, could not be repeated. It is hoped that the reasons for this irreproducibility will be discovered and that the performance of these mixtures will be *recovered*, that is, the mixtures will repeatedly drive a projectile at least 2 m.

Looking at the successful third stage experiment, assuming that the performance can be recovered, one can see the results of applying the high velocity technique. The slope of the velocity-position curve is greater than that of the record experiment, due to a combination of the reduced mass projectile and the higher performance mixtures. Referring to Fig. 6.10, all three stages accelerated the projectile at over 30,000 *g's* after 6 m, whereas the old experiment averaged about 26,000 *g's*. If the second stage performance, 36,000 *g's*, can be recovered, along with the 35,000 *g's* observed in the third

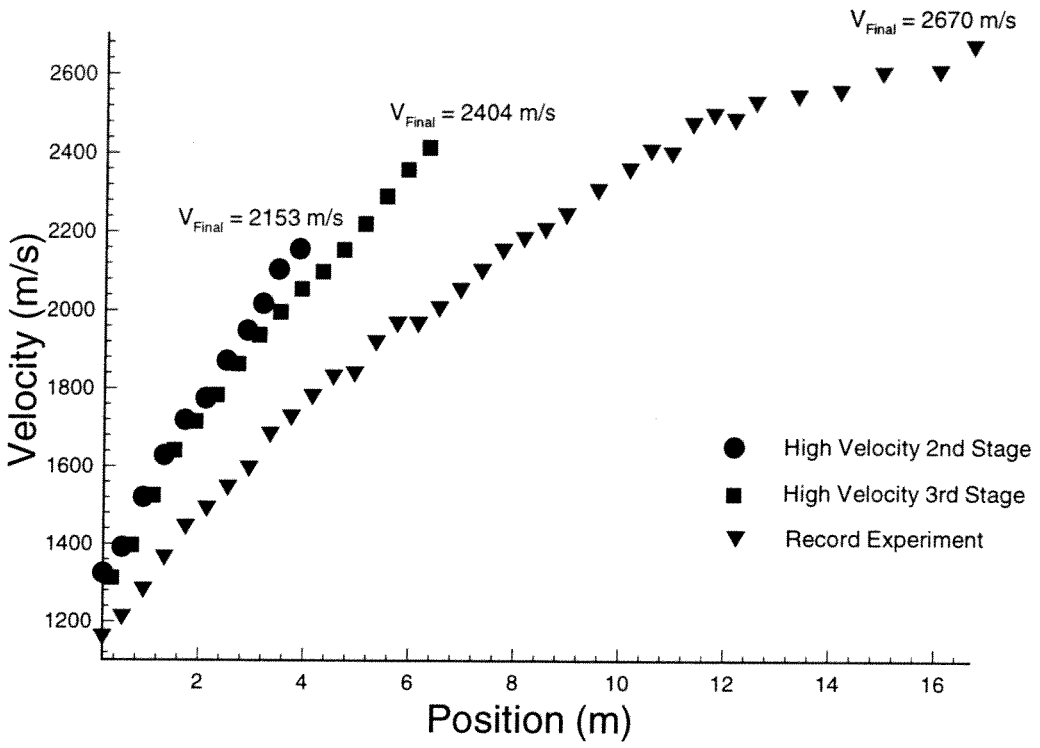


**Figure 6.12: Comparison of high velocity experiments to record experiment.**

stage, then a velocity of 2450 m/s is possible after 6 m. Even without recovered second stage performance, the velocity of about 2400 m/s observed after 6 m in the high velocity third stage experiment was obtained in half the distance it took in the old experiment. Thus, in essence, the effective acceleration distance has been halved. The average acceleration in the successful third stage experiment over 6 m was 34,700 *g's*. If that were to be sustained over the entire 16 m length of the UW ram accelerator, a final velocity of 3550 m/s would result. Clearly, the technique developed is successful at improving ram accelerator performance.

# 7. Conclusions and Recommendations

The motivation of the research presented in this thesis was to develop a technique to obtain high velocity experiments in a relatively few number of experiments and apply that technique, in the hopes of achieving velocities of at least 3 km/s. Thermally choked theory was analyzed and used to determine methods for achieving high accelerations. Experiments were performed which validated these methods.

## 7.1 Conclusions

The basic approach to high velocity can be summarized with two concepts: a) reduce the projectile mass; b) optimize the propellant mixture for highest thrust. The experimental work by Imrich of the UW to determine the impact of projectile geometry on performance was applied to a new design which reduced the mass of an aluminum projectile by about one third, from 75 gm to 50 gm.

Using thermally choked one-dimensional theory, mixture maps were developed which clearly show the relationship between nondimensional heat release, $Q$, and entrance freestream Mach number, $M_{in}$. Knowing the mass, stage length, and entrance velocity of the ram accelerator stage through which the projectile travels, the theoretical acceleration was determined as a function of propellant mixture and overlaid upon the mixture maps, allowing one to quickly determine which mixtures should produce the highest accelerations. Although the thermally choked one-dimensional theory accurately models performance, it does not predict whether or not a projectile will operate in a given mixture. Mixture maps allow limitations in either $Q$ or $M_{in}$ to be quickly discovered and also provide alternative mixtures for high performance.

Repeatable accelerations of over 38,000 *g's* were observed in 2-m stages, and an acceleration of 34,700 *g's* over 6 m was observed in three 2-m stages, although that performance has not been repeated as of this writing. A velocity of 2404 m/s has been observed over 6 m; the record experiment took 12 m to accelerate a projectile to that

velocity. Through the combination of reduced projectile mass and improved propellant combinations, the thermally choked ram accelerator has demonstrated the potential for high velocity.

Great care has been taken in this work to delay making references to specific ram accelerators as long as possible. The technique for high velocity performance is applicable to any ram accelerator that operates in the subdetonative propulsion mode. It is the hope of the author that this technique is applied to realize high velocities at the other facilities worldwide.

## 7.2 Recommendations

The goal of achieving 3 km/s has not been met, but it is far from impossible. The high velocity technique can and should be applied to further stage development. The difficulties described with respect to different stage lengths will hopefully be overcome and performance will be recovered. The ram accelerator is a unique, fascinating concept which, in the opinion of the author, holds tremendous potential as a hypervelocity launcher. The technique and experiments described herein provide some insight into its nature, but there is much more to learn. It is hoped that the maximum observed velocity will increase as research continues, and some of the potential applications of the ram accelerator will be realized.

# References


1. Hertzberg, A., Bruckner, A.P. and Bogdanoff, D.W., "Ram Accelerator: A New Chemical Method for Accelerating Projectiles to Ultrahigh Velocities," *AIAA Journal*, Vol. 26, 1988, pp. 195-203.

2. Sutton, G.P., Rocket Propulsion Elements, Sixth Edition, John Wiley and Sons, 1992, p.1.

3. Hertzberg, A., Bruckner, A.P. and Knowlen, C., "Experimental Investigation of Ram Accelerator Propulsion Modes," *Shock Waves*, Vol. 1, 1991, pp. 17-25.

4. Knowlen, C., Higgins, A.J., Bruckner, A.P. and Bauer, P., "Ram Accelerator Operation in the Superdetonative Velocity Regime," AIAA Paper 96-0098, January 1996.

5. Krucyznski, D., "New Experiments in a 120 mm Ram Accelerator at High Pressures," AIAA Paper 93-2589, June 1993.

6. Bruckner, A.P. and Hertzberg, A., "Ram Accelerator Direct Launch System for Space Cargo," International Astronautical Federation Paper IAF-87-211, October 1987.

7. Hertzberg, A., Bruckner, A.P. and Knowlen, C., "Applications of the Ram Accelerator to Hypervelocity Aerothermodynamic Testing," AIAA Paper 92-3949, July 1992.

8. Seiler, F., Patz, G., Smeets, G. and Srulijes, J., "The Rail Tube in Ram Acceleration: Feasibility Study with ISL's RAMAC 30," Proceedings of the Second International Workshop on Ram Accelerators, University of Washington, Seattle, WA, July 17-20, 1995.

9. Giraud, M., Legendre, J.F., Simon, G., Henner, M. and Voison, D., "RAMAC in 90 mm Caliber of RAMAC 90. Starting Process, Control of the Ignition Location and Performance in the Thermally Choked Performance Mode, Proceedings of the Second International Workshop on Ram Accelerators, University of Washington, Seattle, WA, July 17-20, 1995.

10. Chang, X., Shinomura, Y. and Taki, S., "Preliminary Tests of a Rectangular Bore Ram Accelerator," Proceedings of the Second International Workshop on Ram Accelerators, University of Washington, Seattle, WA, July 17-20, 1995.

11. Sasoh, A. and Takayama, K., "Ramac 25 at Shock Wave Research Center," Proceedings of the Second International Workshop on Ram Accelerators, University of Washington, Seattle, WA, July 17-20, 1995.

12. Higgins, A.J., "Gas Dynamic Limits of the Ram Accelerator," MS Thesis, University of Washington, 1993.

13. Knowlen, C., Higgins, A.J. and Bruckner, A.P., "Investigation of Operational Limits to the Ram Accelerator," AIAA Paper 94-2967, June 1994.

14. Knowlen, C., "Theoretical and Experimental Investigation of the Thermodynamics of the Thermally Choked Ram Accelerator," Ph.D. Dissertation, University of Washington, 1991.

15. Kuo, K. K., *Principles of Combustion*, Wiley, New York, 1986, p. 234.

16. Buckwalter, D., Knowlen, C. and Bruckner, A.P., "Ram Acclerator Performance Analysis Code Incorporating Real Gas Effects," AIAA Paper 96-2945, July 1996.

17. Higgins, A.J., Knowlen, C. and Bruckner, A.P., "An Investigation of Ram Accelerator Gas Dynamic Limits," AIAA Paper 93-2181, June 1993.

18. Imrich, T.S., "The Impact of Projectile Geometry on Ram Accelerator Performance," MS Thesis, University of Washington, 1995.

19. Seigel, A.E., "The Theory of High Speed Guns," AGARDograph 91, North Atlantic Treaty Organization Advisory Group for Aerospace Research and Development, May 1965.

20. Hinkey, J.B., "An Experimental and Numerical Investigation of the Three-Dimensional Flow Field About a Ram Accelerator Projectile," Ph.D. Dissertation, University of Washington, 1994.

21. Seiler, F., and Mathieu, G., "Boundary Layer Model for Calculating the Heat Transfer into a Ram Projectile Fired into a Ram Accelerator," Proceedings of the Second International Workshop on Ram Accelerators, University of Washington, Seattle, WA, July 17-20, 1995.

22. Liberatore, F., "The Effects of Real Material Behavior on Ram Accelerator Performance," Proceedings of the Second International Workshop on Ram Accelerators, University of Washington, Seattle, WA, July 17-20, 1995.

23. Naumann, K.W., "Thermal Stress Due to Aerodynamic Heating of Projectiles During Acceleration in a Ram Accelerator Tube," Proceedings of the Second International Workshop on Ram Accelerators, University of Washington, Seattle, WA, July 17-20, 1995.

24. Chew, G., "Projectile Nose Heating in the Ram Accelerator," Ph.D. Dissertation, University of Washington, 1995.

25. Auzias de Turenne, J., "An Analysis of Ram Accelerator Projectile Materials," AIAA Paper 92-0262, January 1992.

26. Schultz, E., "The Subdetonative Ram Accelerator Starting Process," MS Thesis, University of Washington, 1997.

27. Elvander, J.E., Knowlen, C., and Bruckner, A.P., "High Velocity Performance of the Ram Accelerator," AIAA Paper 96-2675, July 1996.

28. Stewart, J.S., Knowlen, C., and Bruckner, A.P., "Effects of Launch Tube Gases on Starting of the Ram Accelerator", AIAA Paper 97-3175 (pending), July, 1997.

# Appendix B: High Velocity First Stage Shot Data

NOTES

- All shots at 50 atm fill pressure.
- HS1236 used an Al body and Al nose. *All other shots except HS1246* used Al body and Ti nose.
- HS1246 was a repeat of HS1241 using the finless throat (a.k.a. "lawn dart") projectile configuration.

| Shot | Date | 1st Stg Mixture | Stg Length (m) | Proj. Mass (gm) | $V_{In}$ (m/s) | $V_{2m}$ (m/s) | Unstart Location (stn) | Unstart Location (m) |
|---|---|---|---|---|---|---|---|---|
| HS1236 | 5/16/96 | $5.5CH_4+2O_2$ | 8 | 49.23 | 1327 | - | 4-5 | ~1.6 |
| HS1237 | 5/17/96 | $6.5CH_4+2O_2$ | 8 | 49.72 | 1322 | 1679 | - | Drove Out (8m) |
| HS1238 | 5/18/96 | $6CH_4+2O_2$ | 8 | 50.10 | 1327 | 1742 | 17-18 | ~6.8 |
| HS1239 | 5/20/96 | $5.75CH_4+2O_2$ | 8 | 49.88 | 1314 | 1742 | 14-15 | ~5.6 |
| HS1240 | 5/21/96 | $5.5CH_4+2O_2+1H_2$ | 8 | 49.87 | 1314 | - | 2-3 | ~0.8 |
| HS1241 | 5/24/96 | $5CH_4+2O_2+2He$ | 8 | 49.86 | 1319 | 1801 | 10-11 | ~4.0 |
| HS1242 | 5/25/96 | $4.4CH_4+2O_2+2He$ | 8 | 49.82 | 1324 | - | 2-3 | ~0.8 |
| HS1243 | 5/27/96 | $4.7CH_4+2O_2+2He$ | 8 | 49.69 | 1327 | - | 2-3 | ~0.8 |
| HS1244 | 5/28/96 | $4.7CH_4+2O_2+3He$ | 8 | 49.80 | 1317 | - | 3-4 | ~1.2 |
| HS1245 | 5/29/96 | $4.85CH_4+2O_2+2He$ | 8 | 49.73 | 1322 | - | 2-3 | ~0.8 |
| HS1246 | 5/30/96 | $5CH_4+2O_2+2He$ | 8 | 44.78 | 1337 | 1789 | 7-8 | ~3.2 |

# Appendix C: High Velocity Second+ Stage Shot Data

NOTES

- All shots at 50 atm fill pressure.
- All shots used Al body and Al nose.
- Redundant mags were used at stations 10,11,15, and 16. Velocity data from these locations were averaged.

a) All mag data was lost on HS1284.

b) A wave fall-off was observed in HS1285. The velocity peaked between stations 7 and 10 and then decreased.

c) In HS1294, the More On Fuel was reduced in the first stage from 154.5 to 154.3, in an attempt to regain the performance observed in the first stage development. The experiment unstarted upon entry into the second stage.

d) In HS1294, HS1295, HS1296, and HS1299, substandard performance was observed when the second stage length was reduced from 8 m to 2 m. It was theorized that this decrease in performance was due to unchoking of the flow orifices due to reduced fill times.

e) During the second stage fills in the three stage experiments HS1300 - HS1305, the second stage (2 m) and third stage (6 m) were filled simultaneously with the second stage mixture, and then the third stage was vented and evacuated and refilled with the third stage mixture. This purpose of this "fill and spill" method was to lengthen the fill time of the second stage in an attempt to counter the problem described in Note (d).

| Shot | Date | Proj. Mass (gm) | Stg | Mixtures | Stg Length (m) | $V_{In}$ (m/s) | $V_{2m}$ (m/s) | Unstart Location (stn) | Unstart Location (m) | Notes |
|---|---|---|---|---|---|---|---|---|---|---|
| HS1284 | 9/9/96 | 50.18 | 1 | $5CH_4+2O_2+2He$ | 2 | ?? | ?? | 5-6 | ~2.0 | a |
| | | | 2 | $3.3CH_4+2O_2+9.5He$ | 8 | ?? | ?? | | | |
| HS1285 | 9/10/96 | 50.31 | 1 | $5CH_4+2O_2+2He$ | 2 | 1309 | 1757 | Wave fall-off @ 9-10 | ~3.6 | b |
| | | | 2 | $3.8CH_4+2O_2+10He$ | 8 | 1757 | - | | | |
| HS1286 | 9/12/96 | 50.31 | 1 | $5CH_4+2O_2+2He$ | 2 | 1327 | 1777 | 14-15 | ~5.6 | |
| | | | 2 | $3.8CH_4+2O_2+7.8He$ | 8 | 1777 | 2095 | | | |

| Shot | Date | Proj. Mass (gm) | Stg | Mixtures | Stg Length (m) | $V_{In}$ (m/s) | $V_{2m}$ (m/s) | Unstart Location (stn) | Unstart Location (m) | Notes |
|---|---|---|---|---|---|---|---|---|---|---|
| HS1287 | 9/13/96 | 50.32 | 1 | $5CH_4+2O_2+2He$ | 2 | 1314 | 1781 | 12-13 | ~4.8 | |
| | | | 2 | $3.3CH_4+2O_2+7.4He$ | 8 | 1781 | 2163 | | | |
| HS1288 | 9/13/96 | 50.32 | 1 | $5CH_4+2O_2+2He$ | 2 | 1322 | 1773 | 13-14 | ~5.2 | |
| | | | 2 | $3CH_4+2O_2+8.2He$ | 8 | 1773 | 2153 | | | |
| HS1289 | 9/14/96 | 50.21 | 1 | $5CH_4+2O_2+2He$ | 2 | 1309 | 1765 | 7-8 | ~2.8 | |
| | | | 2 | $2.7CH_4+2O_2+8He$ | 8 | 1765 | - | | | |
| HS1290 | 9/16/96 | 50.31 | 1 | $5CH_4+2O_2+2He$ | 2 | 1317 | 1777 | 8-9 | ~3.2 | |
| | | | 2 | $2.9CH_4+2O_2+7.1He$ | 8 | 1777 | - | | | |
| HS1291 | 9/16/96 | 50.04 | 1 | $5CH_4+2O_2+2He$ | 2 | 1307 | 1781 | 12-13 | ~4.8 | |
| | | | 2 | $2.9CH_4+2O_2+8.7He$ | 8 | 1781 | 2190 | | | |
| HS1292 | 9/17/96 | 50.33 | 1 | $5CH_4+2O_2+2He$ | 2 | 1312 | 1781 | 6-7 | ~2.4 | |
| | | | 2 | $2.9CH_4+2O_2+8.7He$ | 8 | 1781 | - | | | |
| HS1293 | 9/17/96 | 50.06 | 1 | $5CH_4+2O_2+2He$ | 2 | 1327 | 1765 | 13-14 | ~5.2 | |
| | | | 2 | $3CH_4+2O_2+8.2He$ | 8 | 1765 | 2112 | | | |

| Shot | Date | Proj. Mass (gm) | Stg | Mixtures | Stg Length (m) | $V_{In}$ (m/s) | $V_{2m}$ (m/s) | Unstart Location (stn) | Unstart Location (m) | Notes |
|---|---|---|---|---|---|---|---|---|---|---|
| HS1294 | 9/21/96 | 50.22 | 1 | $4.98CH_4+2O_2+2He$ | 2 | 1322 | 1789 | 6-7 | ~2.4 | c,d |
| | | | 2 | $3CH_4+2O_2+8.2He$ | 2 | 1789 | - | | | |
| | | | 3 | $2.1CH_4+2O_2+13.6He$ | 6 | - | - | | | |
| HS1295 | 9/23/96 | 50.06 | 1 | $5CH_4+2O_2+2He$ | 2 | 1319 | 1769 | 6-7 | ~2.4 | d |
| | | | 2 | $3CH_4+2O_2+8.2He$ | 2 | 1769 | - | | | |
| | | | 3 | $2.1CH_4+2O_2+13.6He$ | 6 | - | - | | | |
| HS1296 | 9/24/96 | 50.30 | 1 | $4.98CH_4+2O_2+2He$ | 2 | 1319 | - | 4-5 - | ~1.6 | d |
| | | | 2 | $3.8CH_4+2O_2+7.8He$ | 2 | - | - | | | |
| | | | 3 | $2.2CH_4+2O_2+12.3He$ | 4 | - | - | | | |
| HS1297 | 9/25/96 | 50.27 | 1 | $4.98CH_4+2O_2+2He$ | 2 | 1317 | - | 4-5 - | ~1.6 | d |
| | | | 2 | $3CH_4+2O_2+8.2He$ | 8 | - | - | | | |
| HS1298 | 9/26/96 | 50.36 | 1 | $5CH_4+2O_2+2He$ | 2 | 1312 | 1785 | 12-13 | ~4.8 | d |
| | | | 2 | $3CH_4+2O_2+8.2He$ | 8 | 1785 | 2172 | | | |

| Shot | Date | Proj. Mass (gm) | Stg | Mixtures | Stg Length (m) | $V_{In}$ (m/s) | $V_{2m}$ (m/s) | Unstart Location (stn) | Unstart Location (m) | Notes |
|---|---|---|---|---|---|---|---|---|---|---|
| HS1299 | 9/27/96 | 50.32 | 1 | $5CH_4+2O_2+2He$ | 2 | 1309 | 1761 | 11-12 | ~4.4 | d |
| | | | 2 | $3.8CH_4+2O_2+7.8He$ | 2 | 1761 | 1983 | | | |
| | | | 3 | $2.2CH_4+2O_2+12.3He$ | 2 | 1983 | - | | | |
| HS1300 | 9/27/96 | 50.37 | 1 | $5CH_4+2O_2+2He$ | 2 | 1312 | 1781 | 18-19 | ~7.2 | e |
| | | | 2 | $3.8CH_4+2O_2+7.8He$ | 8/2 | 1781 | 2100 | | | |
| | | | 3 | $2.2CH_4+2O_2+12.3He$ | 6 | 2100 | 2404 | | | |
| HS1301 | 9/28/96 | 50.28 | 1 | $5CH_4+2O_2+2He$ | 2 | 1309 | 1781 | 9-10 | ~3.6 | e |
| | | | 2 | $3CH_4+2O_2+8.2He$ | 8/2 | 1781 | - | | | |
| | | | 3 | $2.3CH_4+2O_2+14.5He$ | 6 | - | - | | | |
| HS1302 | 9/29/96 | 50.23 | 1 | $5CH_4+2O_2+2He$ | 2 | 1305 | 1765 | 13-14 | ~5.2 | e |
| | | | 2 | $3.5CH_4+2O_2+7.6He$ | 8/2 | 1765 | 2120 | | | |
| | | | 3 | $2.3CH_4+2O_2+13.7He$ | 6 | 2120 | - | | | |
| HS1303 | 9/30/96 | 50.34 | 1 | $5CH_4+2O_2+2He$ | 2 | 1307 | 1777 | 7-8 | ~2.8 | e |
| | | | 2 | $3.5CH_4+2O_2+7.6He$ | 8/2 | 1777 | - | | | |
| | | | 3 | $2.2CH_4+2O_2+12.3He$ | 6 | - | - | | | |

| Shot | Date | Proj. Mass (gm) | Stg | Mixtures | Stg Length (m) | $V_{In}$ (m/s) | $V_{2m}$ (m/s) | Unstart Location (stn) | Unstart Location (m) | Notes |
|---|---|---|---|---|---|---|---|---|---|---|
| HS1304 | 9/30/96 | 50.27 | 1 | $5CH_4+2O_2+2He$ | 2 | 1330 | 1769 | 12-13 | ~4.8 | e |
| | | | 2 | $3.8CH_4+2O_2+7.8He$ | 8/2 | 1769 | 2046 | | | |
| | | | 3 | $2.2CH_4+2O_2+12.3He$ | 6 | 2046 | - | | | |
| HS1305 | 10/1/96 | 50.37 | 1 | $5CH_4+2O_2+2He$ | 2 | 1324 | 1765 | 10-11 | ~4.0 | e |
| | | | 2 | $3.8CH_4+2O_2+7.8He$ | 8/2 | 1765 | - | | | |
| | | | 3 | $2.5CH_4+2O_2+12.4He$ | 6 | - | - | | | |

# Appendix A: Mixture Maps

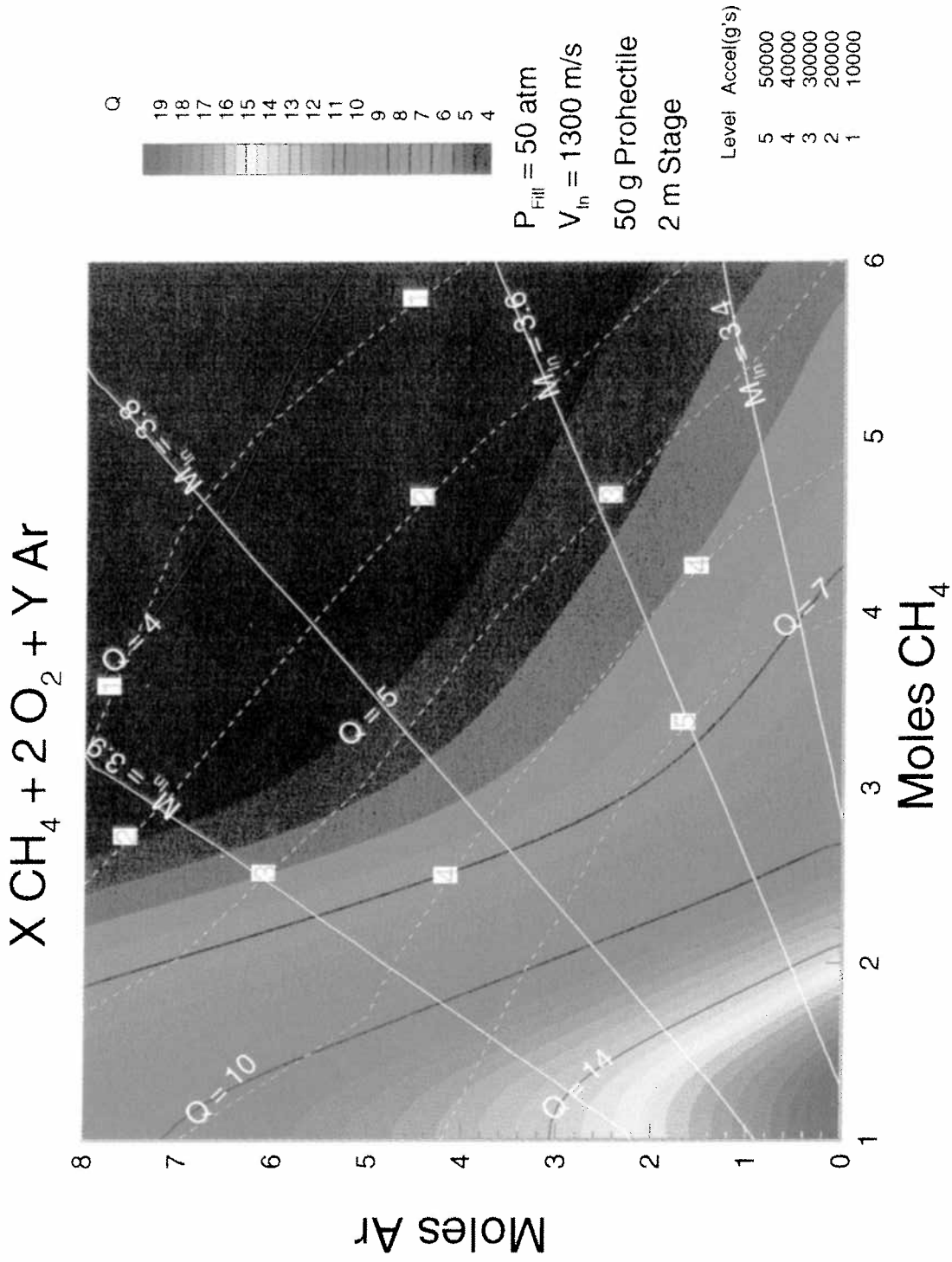

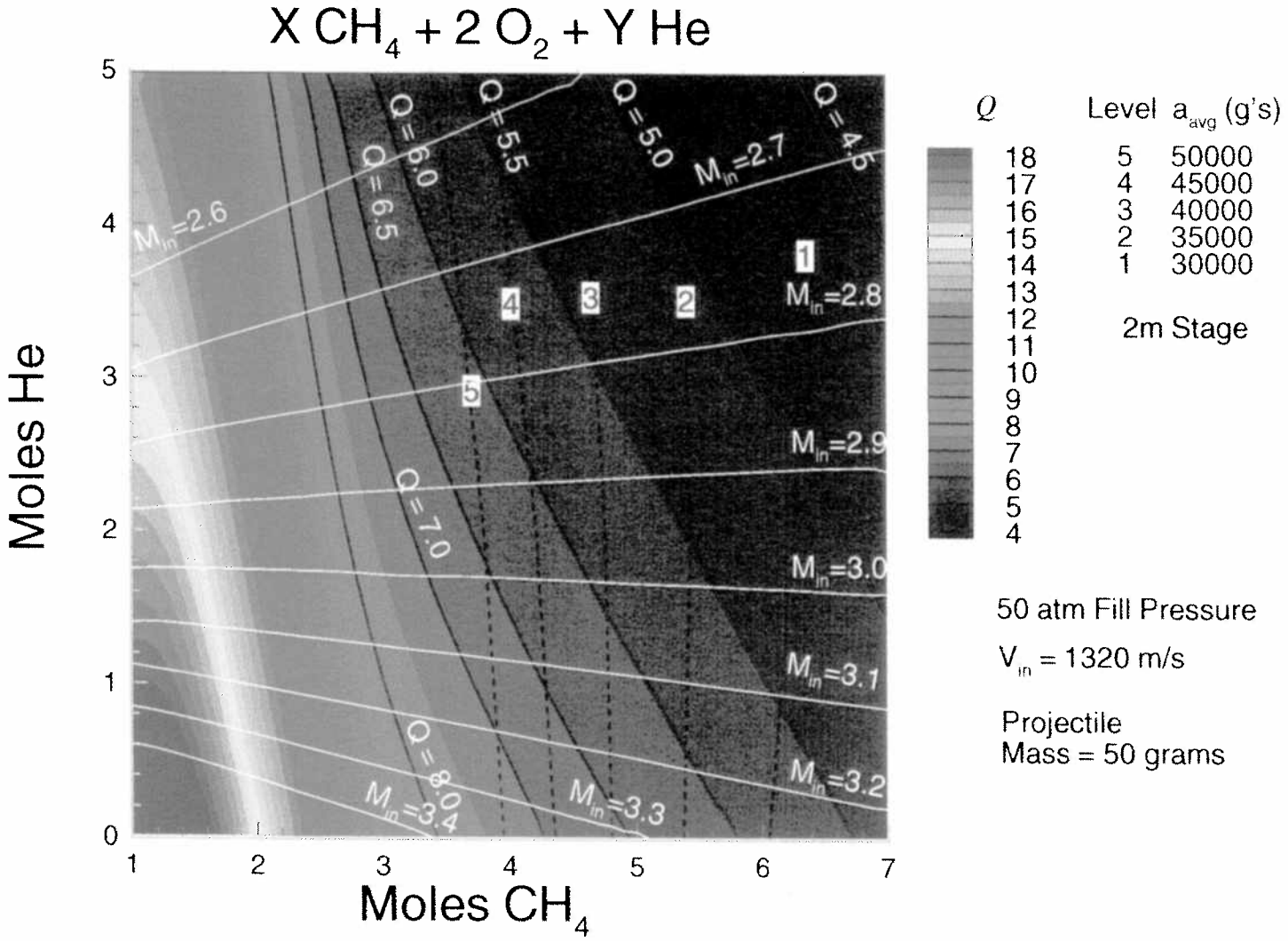
X CH4 + 2 O2 + Y He
Moles He
Moles CH4
Q = 6.0
Q = 5.5
Q = 5.0
Q = 4.5
Q = 6.5
Q = 7.0
Q = 8.0
M_in=2.6
M_in=2.7
M_in=2.8
M_in=2.9
M_in=3.0
M_in=3.1
M_in=3.2
M_in=3.3
M_in=3.4
1
2
3
4
5
Q
18
17
16
15
14
13
12
11
10
9
8
7
6
5
4
Level a_avg (g's)
5 50000
4 45000
3 40000
2 35000
1 30000
2m Stage
50 atm Fill Pressure
V_in = 1320 m/s
Projectile
Mass = 50 grams

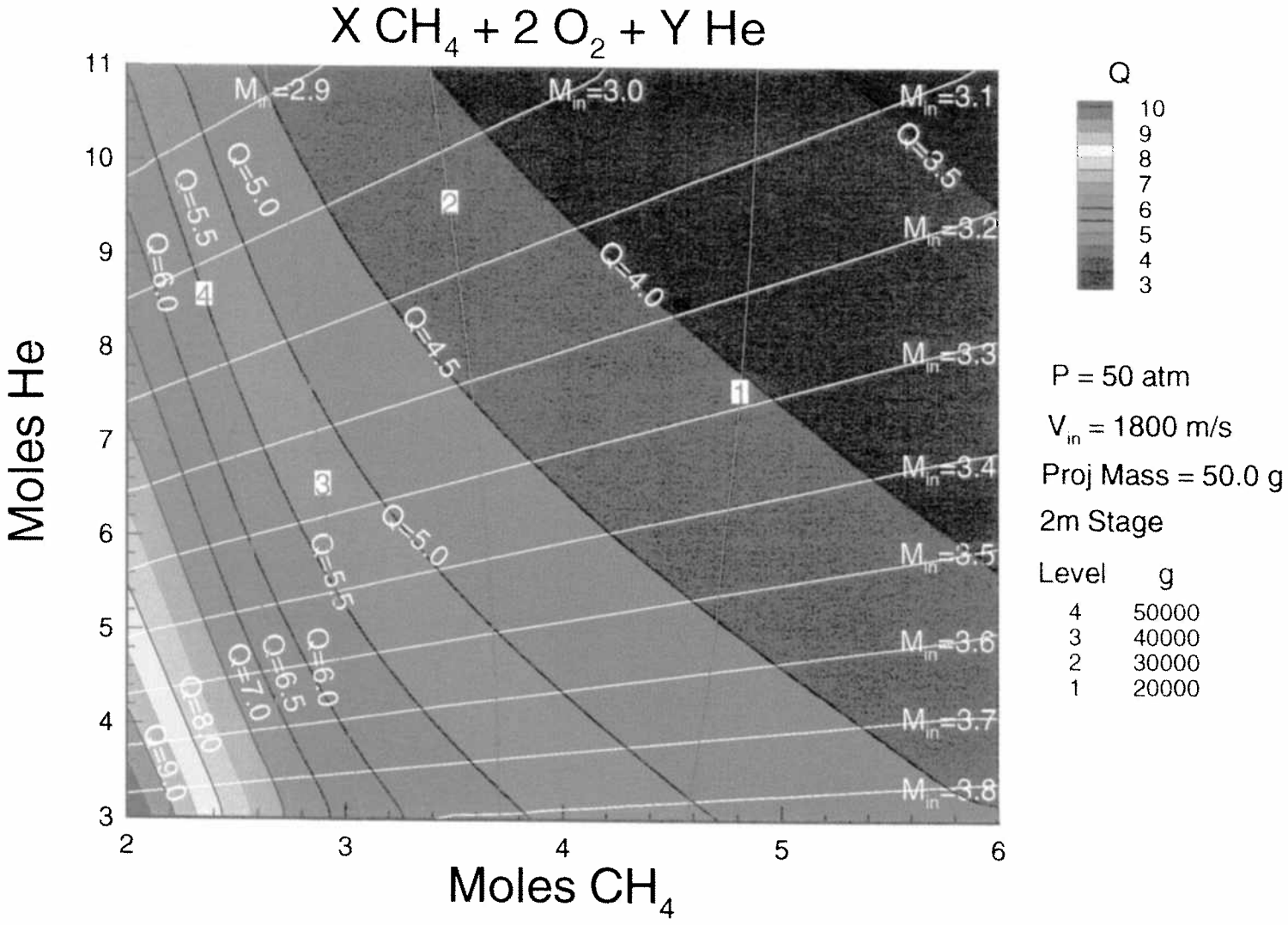
X CH4 + 2 O2 + Y He
Moles He
Moles CH4
11
10
9
8
7
6
5
4
3
2
3
4
5
6
Min=2.9
Min=3.0
Min=3.1
Min=3.2
Min=3.3
Min=3.4
Min=3.5
Min=3.6
Min=3.7
Min=3.8
Q=3.5
Q=4.0
Q=4.5
Q=5.0
Q=5.5
Q=6.0
Q=6.5
Q=7.0
Q=8.0
Q=9.0
1
2
3
4
Q
10
9
8
7
6
5
4
3
P = 50 atm
Vin = 1800 m/s
Proj Mass = 50.0 g
2m Stage
Level g
4 50000
3 40000
2 30000
1 20000

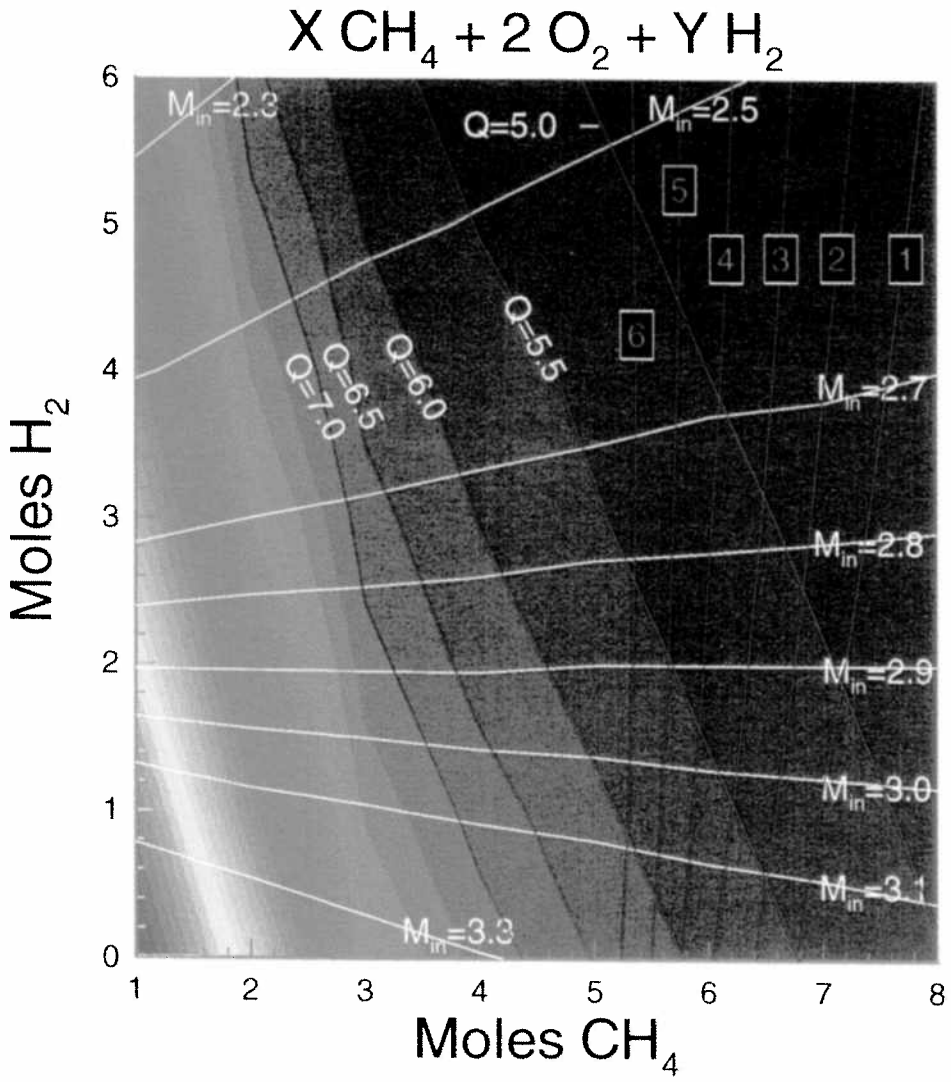


| Q | Level | $a_{avg}$ (g's) |
|---|---|---|
| 20.0 | 6 | 37000 |
| 19.0 | 5 | 35000 |
| 18.0 | 4 | 33000 |
| 17.0 | 3 | 31000 |
| 16.0 | 2 | 29000 |
| 15.0 | 1 | 27000 |
| 14.0 | | |
| 13.0 | | |
| 12.0 | | |
| 11.0 | | |
| 10.0 | | |
| 9.0 | | |
| 8.0 | | |
| 7.0 | | |
| 6.0 | | |
| 5.0 | | |
| 4.0 | | |

50 atm

$V_{in}$ = 1320 m/s

Projectile Mass = 50 grams

2 m Stage

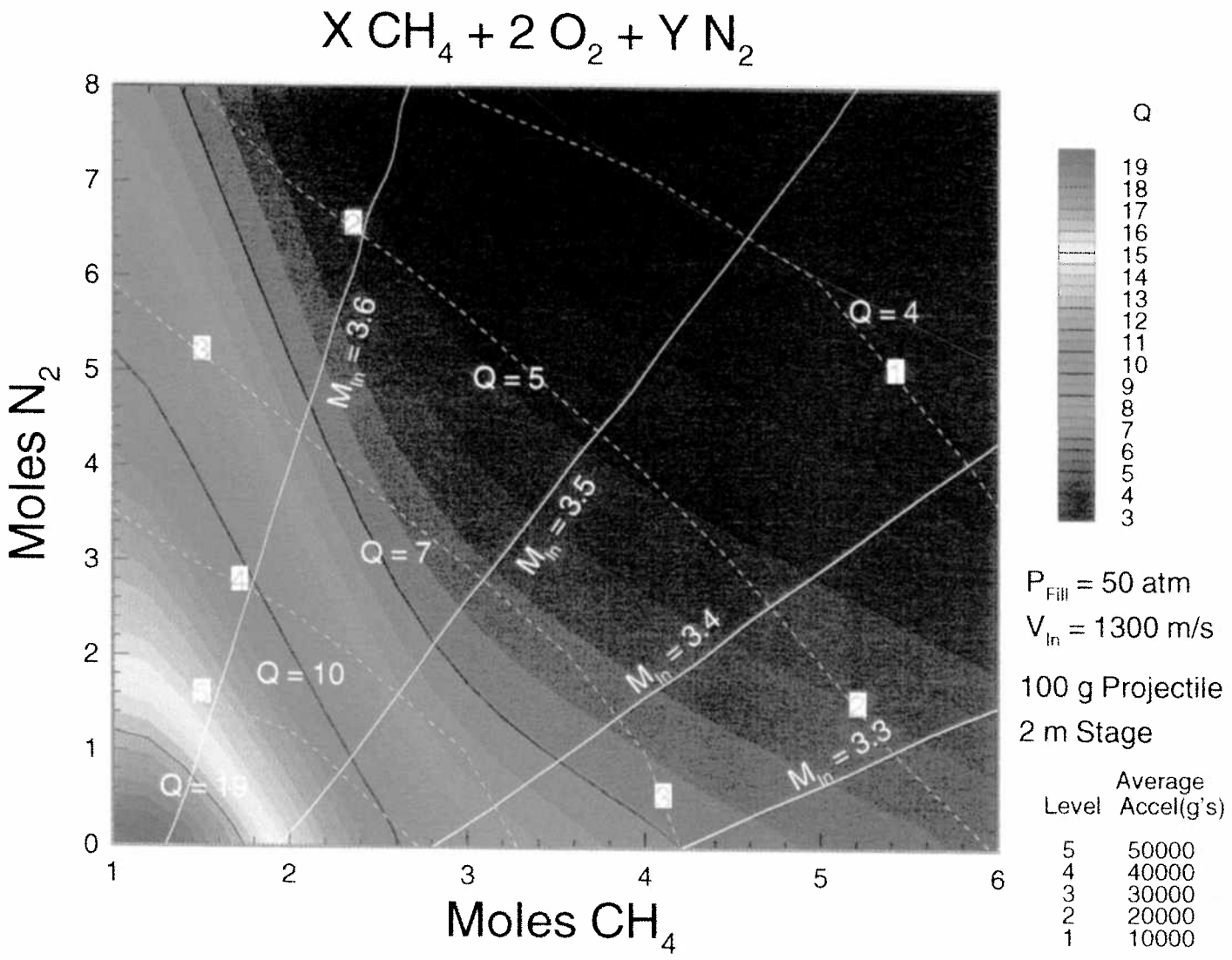
X CH4 + 2 O2 + Y N2
Moles N2
Moles CH4
Q
19
18
17
16
15
14
13
12
11
10
9
8
7
6
5
4
3
Q = 4
Q = 5
Q = 7
Q = 10
Q = 19
Min = 3.6
Min = 3.5
Min = 3.4
Min = 3.3
PFill = 50 atm
Vin = 1300 m/s
100 g Projectile
2 m Stage
Level
Average Accel(g's)
5 50000
4 40000
3 30000
2 20000
1 10000